Cloud Cover and Climate Sensitivity

RICHARD T. WETHERALD AND SYUKURO MANABE

Geophysical Fluid Dynamics Laboratory/NOAA, Princeton University, Princeton, N.J. 08540

(Manuscript received 12 September 1979, in final form 25 March 1980)

ABSTRACT

This study discusses how the sensitivity of climate may be affected by the variation of cloud cover based on the results from numerical experiments with a highly simplified, three-dimensional model of the atmospheric general circulation. The model explicitly computes the heat transport by large-scale atmospheric disturbances. It contains the following simplifications: a limited computational domain, an idealized geography, no heat transport by ocean currents and no seasonal variation. Two versions of the model are constructed. The first version includes prognostic schemes of cloud cover and its radiative influences, and the second version uses a prescribed distribution of cloud cover for the computation of radiative transfer. Two sets of equilibrium climates are obtained from the long-term integrations of both versions of the model for several values of the solar constant. Based on the comparison between the variable and the fixed cloud experiments, the influences of cloud cover variation on the response of a model climate to an increase of the solar constant are identified.

It is found that, in response to an increase of the solar constant, cloudiness diminishes in the upper and middle troposphere at most latitudes and increases near the earth's surface and the lower stratosphere of the model particularly in higher latitudes. Because of the changes described above, the total cloud amount diminishes in the region equatorward of 50° latitude with the exception of a narrow subtropical belt. However, it increases in the region poleward of this latitude. In both regions, the area mean change in the net incoming solar radiation, which is attributable to the cloud-cover change described above, is approximately compensated by the corresponding change in the outgoing terrestrial radiation at the top of the model atmosphere. For example, equatorward of 50° latitude, the reduction of both cloud amount and effective cloud-top height contributes to the increase in the area-mean flux of outgoing terrestrial radiation and compensates for the increase in the flux of net incoming solar radiation caused by the reduction of cloud amount. Poleward of 50° latitude, the increase of cloudiness contributes to the reduction of both net incoming solar and outgoing terrestrial fluxes at the top of the model atmosphere. Although the effective cloud-top height does not change as it does in lower latitudes, the changes of these fluxes approximately compensate each other because of the smallness of insolation in high latitudes. Owing to the compensations mentioned above, the changes of cloud cover have a relatively minor effect on the sensitivity of the area-mean climate of the model.

1. Introduction

Using mathematical models of climate with varying degrees of sophistication, various investigators have attempted to evaluate the response of climate to external or internal stimuli, such as changes of the solar constant or in the CO_2 content of the atmosphere (e.g., Manabe and Wetherald, 1967; Schneider, 1975). One of the important assumptions adopted in these studies is that the distribution of cloud cover is independent of these stimuli. Unfortunately, it is far from obvious that the distribution of cloud cover remains unchanged despite the change in the atmospheric state resulting from the application of a stimulus. Since cloud cover exerts a strong influence on the radiation field in the atmosphere, it is desirable to investigate how the cloud feedback mechanism (i.e., the interaction among atmospheric circulation, cloud cover and radiation) affects the response of climate to an external stimulus such as a change in the solar constant. The major objective of this study is to investigate the specific nature of the cloud feedback mechanism and its role in determining the sensitivity of climate.

It is expected that cloud cover exerts two opposing influences upon climate. On the one hand, cloud cover reflects solar radiation and exerts a cooling effect on climate. On the other hand, it reduces the effective temperature for outgoing terrestrial radiation and contributes to the warming of climate. (Note that cloud-top temperature is usually colder than the temperature of the earth's surface.) Based on the study with a radiative, convective equilibrium model of the atmosphere, Manabe and Wetherald (1967) suggested that low cloud has a strong net cooling effect on climate because of the high surface albedo and relatively high cloud-top temperature. On the other hand, their results indicate that high clouds have either a weak

cooling (or heating) effect on climate because of a small albedo and relatively low cloud-top temperature. Nevertheless, their results indicate that the overall effect of cloud cover on climate is cooling. Schneider (1972) reached a similar conclusion in his study of the influences of cloud cover on the radiation balance of the earth-atmosphere system. These results may lead one to speculate that the larger the cloud amount is, the stronger is its cooling effect. However, this may not be necessarily so, because the change in cloud amount is often accompanied by a change in cloud height which results in the change in the radiative balance of the atmosphere-earth system as discussed, for example, by Schneider (1972). The radiative effect of the simultaneous changes of both amount and height of cloud cover is the subject of an extensive discussion in this paper.

Various speculations have been made on the influence of the cloud variation on the sensitivity of climate. For example, in his discussion of the climate effect of the increase of carbon dioxide in the atmosphere, Smagorinsky (1978) speculated that the increase in downward radiative flux due to the addition of carbon dioxide, enchances evaporation from the earth's surface, increases the amount of low cloud and thus exerts a cooling effect on climate. In short, he suggested that the possible warming effect of the CO_2 increase may be compensated by this negative feedback process. On the other hand, the recent studies of Roads (1978) and Schneider *et al.* (1978) indicate that cloud variation may have a positive feedback effect on the sensitivity of the global mean climate. Both studies discuss the response of cloud cover to an increase of sea surface temperature based on the results from numerical experiments with general circulation models of the atmosphere. For example, Roads' analysis indicates that the warmer the sea surface temperature, the larger are the variance of vertical velocity and the efficiency of moisture removal through precipitation. This results in a lower relative humidity, a smaller cloudiness and a smaller reflection of solar radiation and further warming of the earth's surface. In short, his results appear to imply that the direction of the cloud feedback mechanism is positive.

The numerical experiments of Wetherald and Manabe (1975), conducted earlier with a simple general circulation model with a fixed distribution of cloud, reveals that relative humidity increases in the lower model troposphere but decreases in the middle and upper troposphere of the model in response to an increase of the solar constant. (Hereafter, this study is referred to as WM75.) This result appears to suggest that both the positive and negative feedback mechanisms mentioned above can operate in the model atmosphere. Recent observational studies of Budyko (1977) and Cess (1976) indicate that the influence of cloud cover on the sensitivity of climate is relatively small, implying that these two processes may effectively counteract each other.

This study represents an attempt to investigate the nature of cloud feedback mechanisms with a simple model of the atmospheric general circulation in which the distribution of cloud cover is a prognostic variable. The response of the climatic equilibrium of the model to an increase of the solar constant is compared with the corresponding response of another model with a fixed cloud cover. In the absence of reliable information on the details of large-scale cloud formation processes, the cloud prediction scheme is constructed to be as simple as possible for ease of interpretation of the results of the numerical experiments. In this connection, it should be noted that the main emphasis of this study is not on the quantitative estimate of the contribution of cloud feedback mechanisms to the sensitivity of climate, but on the investigation of the specific nature of this contribution.

2. Model structure

a. Basic equations

The general circulation model used for this study includes the prognostic equations of wind, surface pressure, temperature and water vapor mixing ratio, which are written in finite-difference forms on a spherical coordinate system. They are the equations of motion, equation of mass continuity, the thermodynamical equation and the continuity equation for water vapor.

Using the so-called hydrostatic approximation, one may write the equations of motion in a simplified form in which only horizontal wind components are prognostic variables. As suggested by Phillips (1957), the vertical coordinate is chosen to be sigma, i.e., pressure normalized by surface pressure. This sigma coordinate system is introduced because it enables one to incorporate the dynamical effect of an uneven lower boundary (i.e., mountains) in a straightforward manner. The equation of motion explicitly computes the contribution of momentum exchange due to large-scale flow, whereas it evaluates the momentum exchange by subgrid-scale eddies through a nonlinear viscosity formulation proposed by Smagorinsky (1963). The vertical mixing of momentum by subgrid-scale eddies in a planetary boundary layer is parameterized in a very simple manner as described by Smagorinsky *et al.* (1965). The corresponding vertical mixing in the free atmosphere is assumed to be zero in view of our ignorance of this process.

The thermodynamical equation computes the rate of temperature change due to the three-dimen

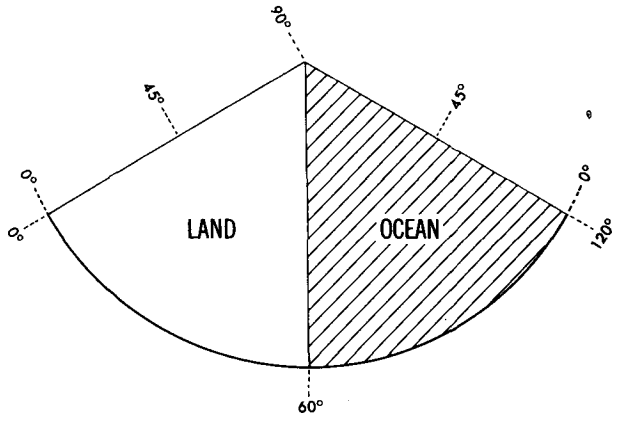

FIG. 1. Computational domain of the model. The oceanic region is hatched.

sional advection of temperature by the large-scale flow, adiabatic compression, radiation, horizontal mixing by subgrid-scale eddies, vertical mixing by forced subgrid-scale eddies in the planetary boundary layer, and a dry and moist convective adjustment.

The continuity equation of water vapor predicts the rate of change of the mixing ratio of water vapor, taking into consideration the effect of three-dimensional advection by the large-scale flow, horizontal mixing by subgrid-scale eddies, vertical mixing by forced subgrid-scale eddies in the planetary boundary layer, and a moist convective adjustment and convective and nonconvective condensation.

b. *Finite-difference equations*

The finite-difference versions of the prognostic equations, mentioned above, are written in such a way that the mass integrals of the square of prognostic variables are unaffected by the contribution of the advection term. This version of the quadratic conservation equation was proposed by Lilly (See the Appendix of Smagorinsky *et al.* 1965) and was further generalized by Bryan (1966). The specific details of the finite-difference representation of the prognostic equations are described by Manabe *et al.* (1975). For the finite-difference computation, a regular latitude-longitude grid system is used. The zonal and meridional grid size are chosen to be 4.5 and 5.0°, respectively. In high-latitude regions of the model where the zonal grid size is small, short zonal wave components contained in each prognostic variable are removed by a Fourier filter so that linear computational instability is prevented in numerical time integration of the prognostic equations. [For further details of this Fourier filter, refer to the paper by Manabe *et al.* (1975).]

In the vertical direction, nine finite-difference levels are chosen in such a way that the model can represent the structures of the stratosphere and planetary boundary layer as well as that of the troposphere. (For approximate pressures at the nine finite-difference levels, see, for example, Fig. 2.)

c. *Computational domain*

To reduce computer time, the computational domain is chosen to be one-third of a hemisphere. It is assumed that fields of all variables are symmetric at the equator and are cyclically continuous between the two boundary meridians which are 120° longitude apart. Furthermore, it is assumed that the model has a highly idealized geography in which two equal areas of continent and ocean divide the computational domain as indicated in Fig. 1. Here, one should note that the oceanic part of the model is highly idealized and does not deal with the dynamics of ocean circulation. The model ocean is a wet surface without any heat capacity. It resembles the actual ocean in that it is wet and is a supplier of moisture to the atmosphere, but it differs from the real ocean because it does not transport heat horizontally or have any heat capacity.

d. *Radiative transfer*

The scheme for computing radiative heating and cooling consists of two parts, i.e., the solar radiation part, and the terrestrial radiation part. The transfer of terrestrial radiation is computed by a method which was originally developed by Rodgers and Walshaw (1966) and was modified by Stone and Manabe (1968). The scheme for computing solar heating of the atmosphere is identical with that described by Manabe and Strickler (1964) and Manabe and Wetherald (1967), except that the entire solar spectrum is split into two subintervals, i.e., infrared range and shorter wave range.

The latitudinal distribution of annual mean insolation is computed assuming the present value of orbital parameters of the earth. The atmospheric absorbers, which are taken into consideration in the computation of radiative transfer, are water vapor, carbon dioxide, ozone and cloud cover. The distribution of water vapor and cloud cover is determined by the prognostic system of the model. The optical properties of cloud are prescribed depending upon the thickness and altitude of cloud as described later in this section. The carbon dioxide concentration is assumed to have a constant mixing ratio (by weight) of 0.456×10^{-3} g g^{-1} of air everywhere in the model atmosphere. An observed annual mean distribution of ozone which varies with respect to latitude and height is prescribed for this study based on the data from Hering and Borden (1965).

TABLE 1. Height range (km), reflectivity (%) and absorptivity (%) of cloud used in this study. λ: wavelength.

Cloud type	Approximate height range (km)	Visible and ultraviolet ($\lambda < 0.7$ μm)		Near infrared ($\lambda > 0.7$ μm)	
		Reflectivity	Absorptivity	Reflectivity	Absorptivity
Thin clouds: high	$10.5 \sim \infty$	21	0	19	4
Thin clouds: middle	$4.0 \sim 10.5$	45	0	35	20
Thin clouds: low	$0 \sim 4.0$	57	0	47	30
Thick clouds		57	0	47	30

e. Moist convection and condensation

The process of moist convection is parameterized using a so-called "moist convective adjustment" proposed by Manabe *et al.* (1965). In this scheme, moist convection takes place when the lapse rate becomes supermoist adiabatic and air exceeds saturation. It is assumed that, in the moist convective layer, the intensity of moist free convection is strong enough to eliminate the vertical gradient of potential temperature instantaneously, while conserving total moist static energy. It is further assumed that the relative humidity in the layer is maintained at 100% owing to the vertical mixing of moisture, condensation, and the evaporation from water droplets. This mechanism of moist convective adjustment represents an extreme idealization of the actual process and does not necessarily reproduce what happens in the actual moist convective layer. For example, it is well known that moist convection can occur when the large-scale relative humidity is less than 100% or that a supermoist adiabatic lapse rate is sometimes maintained in a moist convective layer. Nevertheless, the moist convective adjustment contains some of the essential mechanisms of moist convection, i.e., neutralization of lapse rate and precipitation of moisture. Above all, it is important to recognize that this process prevents the so called convective instability of the first kind which gives rise to grid scale convection unresolvable by a finite-difference representation in the model atmosphere.

When the air tends to become super-saturated, but the static stability is submoist adiabatic, it is assumed that nonconvective condensation takes place reducing humidity to 100% and releasing latent heat.

f. Determination of cloud cover and its optical properties

As pointed out already, the scheme of cloud prediction was chosen to be as simple as possible. It assumes that cloud cover exists wherever condensation takes place. A cloud amount of 80% is assigned to condensation, which occurs at a single or at multiple contiguous finite-difference levels. In the latter case, the cloud cover is regarded as a thick cloud. At all grid points where condensation does not occur the cloud amount is assumed to be zero. The value of 80% mentioned above is chosen so that the model atmosphere will equilibrate at a realistic temperature by maintaining a realistic area mean cloud amount.

In the prognostic system of water vapor and cloud cover described above, a cloud does not correspond to liquid water suspended in the model atmosphere. For the sake of simplicity, it is assumed that all condensed water vapor immediately precipitates, though cloud cover is predicted wherever and whenever condensation takes place.

The fractional absorption and reflection of solar radiation by various types of cloud cover are chosen subjectively referring to the results from the measurements of Drummond and Hickey (1971). They are tabulated in Table 1 where "thin cloud" indicates a cloud which occupies only one finite-difference level and thick cloud occupies more than one contiguous finite-difference level. In this table, optical parameters are given for two spectral ranges, i.e., the near-infrared and the shorter wavelength (i.e., visible and ultraviolet). The value for each spectral range is determined from the optical parameter for the entire solar spectrum using the method suggested by Rodgers (1967). Table 1 indicates the altitude range where each thin cloud is located.

In constructing this table, it is assumed that all thick clouds have both reflectivity and absorptivity, which are similar to those of low cloud, regardless of their altitude. For the computation of terrestrial radiation, all clouds are assumed to be completely black.

Since the optical properties of clouds chosen for this study are highly idealized, they may be significantly different from reality. For example, thin high cloud may not act as a blackbody for terrestrial radiation. Or, the solar reflectivity of thick cloud may be larger than the value assumed for the present study. Therefore, it is necessary to evaluate how the sensitivity of the model climate is affected by the choice of the values of the optical parameters of cloud. The results from such an evaluation are discussed in Section 5d.

g. Heat balance of earth's surface

The temperature of the continental and oceanic surfaces are determined in such a way that they satisfy a condition of heat balance. For simplicity, it is assumed that the earth's surface has no heat capacity. Accordingly, the condition of heat balance requires that the contributions of solar and terrestrial radiation and those of sensible and latent heat flux locally add to zero. The surface temperature which satisfies this heat balance condition is computed numerically with an iteration technique. The assumption of a zero surface heat capacity adopted in this study could have caused the exaggeration of the amplitudes of diurnal and seasonal variation in surface temperature. However, the removal of the diurnal as well as seasonal component from the insolation of the model eliminates this possibility.

For the computation of the heat balance of the earth's surface, it is necessary to specify the distribution of surface albedo. The albedos of both continental and oceanic surfaces are specified as functions of latitude but are assumed to be independent of longitude. For further details of the data source, see Fig. 1 of Manabe (1969). The albedos of snowcover and sea ice are assumed to be 45 and 35%, respectively, when the surface temperature is above -10°C, whereas both surfaces are assumed to have albedos of 70% when the surface temperature falls below -10°C.

h. Ground hydrology

The schemes for computing the hydrology of the ground surface are similar to those described by Manabe (1969). In this scheme, the rate of change in soil moisture is computed as a net contribution from rainfall, snowmelt and evaporation. Runoff is predicted at a grid point when a computed soil moisture exceeds the field capacity of soil, assumed to be 15 cm at all land points for the sake of simplicity.

The effect of soil moisture on evaporation is incorporated into the model by a simple scheme used by Budyko (1958). When the soil does not contain a sufficient amount of water, the amount of evaporation is smaller than that from a perfectly wet surface. If the soil moisture is greater than a certain critical percentage (75% in this study) of the maximum soil capacity, evaporation is assumed to equal the maximum rate. Otherwise, evaporation from land is computed to be linearly proportional to soil moisture up to this critical value.

The rate of change of water equivalent depth of snow is computed as the difference between the rate of snowfall and the sum of the rate of snowmelt and that of sublimation. Precipitation, which is obtained from the prognostic system of water vapor mentioned earlier, is regarded as snowfall if the temperature at a height of 350 m is below freezing. The rate of sublimation is computed in a manner similar to the computation of the evaporation rate from a wet surface except that saturation vapor pressure over ice (instead of water) is used as a surface condition. The snowmelt rate is calculated from a surface heat budget under the assumptions that the temperature of the snow surface does not exceed the freezing point and that the conductivity of snow is zero.

TABLE 2. The list of numerical experiments conducted in this study and the value of solar constant assumed for each experiment.

Variable cloud experiments	Fixed cloud experiments	Solar constant (W m^{-2})	Fraction
VCS	FCS	1444	1.00
VC2	FC2	1472	1.02
VC4	FC4	1500	1.04
VC6	FC6	1528	1.06

3. Plan of numerical experiment

In this study, two series of numerical experiments are conducted. First, quasi-equilibrium climates are obtained for various values of the solar constant from the time integration of a version of the model in which cloud cover is a predicted variable. This set of experiments is called "variable cloud experiments." Second, another series of experiments for the same set of solar constants are carried out with a version of the model in which a fixed set of given distributions of cloud cover is assumed. The second series of experiments are called "fixed cloud experiments." By comparing the two sets of climates, which are obtained from these two sets of experiments, it is expected to determine the influence of cloud feedback on the sensitivity of the model climate.

The values of the solar constant used for both series of experiments are 1444, 1472, 1500 and 1528 W m^{-2}. These values are somewhat higher than the normal value, i.e., 1395 W m^{-2}. Because of the bias of the model,[1] the model atmosphere with the normal value of the solar constant tends to equilibrate at too low a surface temperature. Therefore, relatively high values of the solar con-

[1] The bias of the model results partly from the fact that the model tends to exaggerate the amount of low cloud which lowers the temperature of the model atmosphere because of its high reflectivity of solar radiation. (Refer to Section 4d which compares the computed and observed distributions of cloud cover.) Although one can identify several possible reasons for the bias of the present model, this overestimation of low cloud is the main reason why the present model equilibrates at a significantly lower temperature than the model of Wetherald and Manabe (1975).

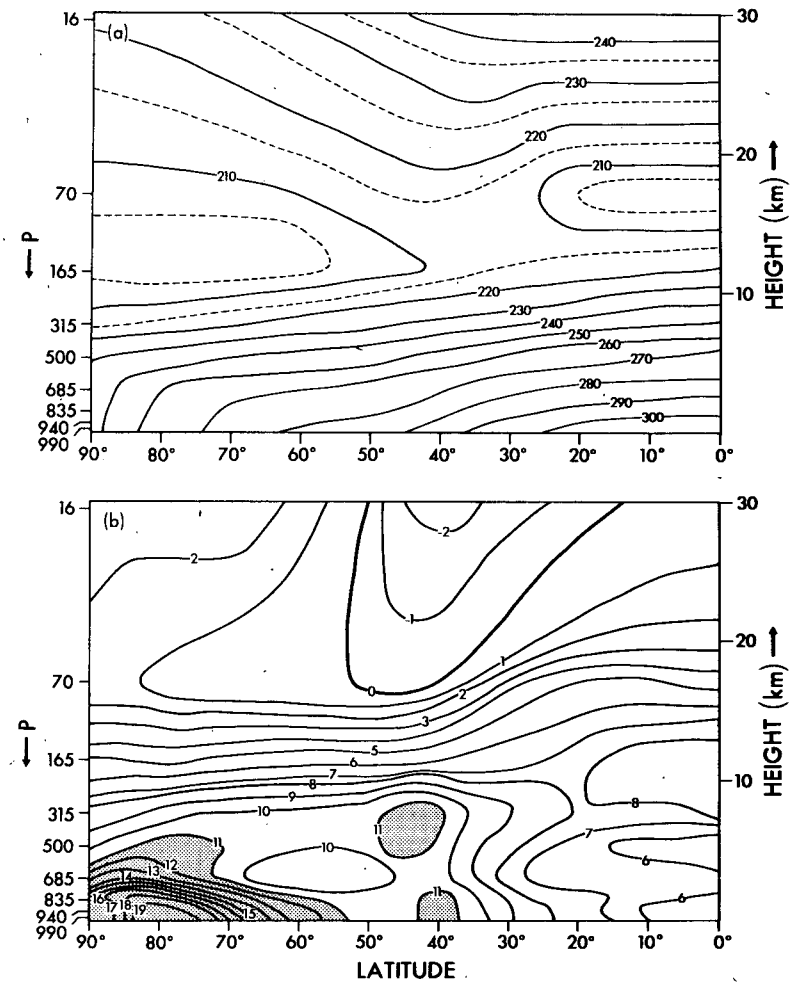

FIG. 2. (a) Latitude-height distribution of zonal-mean temperature in the VCS atmosphere. (b) Latitude-height distribution of zonal-mean temperature difference between the VC6 and VCS atmosphere. Units are in K.

stant are chosen for the present numerical experiments. In this paper, the experiments which assume the solar constant of 1444 W m^{-2} are called standard experiments and are identified by the alphabet character S. The remaining experiments, in which the solar constant is larger than the standard experiment by 2, 4 and 6% are identified by numerals 2, 4 and 6, respectively. Table 2 shows the abbreviated names and the assumed values of the solar constant for all experiments which are conducted in this study. Here, VC and FC stand for Variable Cloud and Fixed Cloud Experiment, respectively.

For the four FC experiments, an identical set of 10 cloud distributions is repeatedly used throughout the course of each time integration. The set represents a random choice from the time series of cloud distributions which are generated by the VCS experiments. This choice of the cloud set for the FC experiments guarantees that the temperature distribution of the FCS atmosphere is not very different from that of the VCS atmosphere and facilitates the intercomparison of the results from the two series of experiments.

The period of the numerical time integration is chosen to be approximately 1200 days for most of the experiments. According to Manabe and Wetherald (1975), this period for time integration is sufficiently long that the uncertainty due to the failure of the model to reach a perfect equilibrium state is much smaller than the climatic response to the small percentage change in the solar constant. Unless otherwise specified, all results presented in this paper represent the time mean state of the model atmosphere during the last 500 days of integration. Again, this period is chosen in such a way that the standard deviation of the variation in the time-mean state is much smaller than the change of the model climate in response to the small percentage change in the solar constant.

4. Response of the VC model

This section briefly describes the response of the VC atmosphere to an increase of the solar constant, and precedes Section 5 where the influence of cloud feedback mechanisms on the sensitivity of the model climate is discussed by comparing the responses of the VC and FC model atmospheres to an increase of the solar constant. Recently, Manabe and Wetherald (1980) investigated the sensitivity of climate to an increase in CO_2 content of air with a model identical to the VC model described in Section 2. They found that the response of the VC model troposphere to a 2% (or 4%) increase of the solar constant resembles the corresponding response to doubling (or quadrupling) the CO_2 content, and discussed the basic causes for this similarity. It is recommended that the reader refer to this companion paper, hereafter referred to as MW80, for a more extensive discussion of the sensitivity of the VC model climate.

a. Temperature

Fig. 2b illustrates the latitude-height distribution of zonal-mean temperature difference between the VC6 and VCS atmospheres. As a reference, the zonal-mean temperature distribution of the VCS atmosphere is added to the upper half of the figure (Fig. 2a). According to this figure, the meridional temperature gradient in the lower model troposphere is significantly reduced in response to the increase of the solar constant. As pointed out by MW80, this reduction is caused by the poleward retreat of the highly reflective snowcover and the marked increase in the poleward transport of latent heat, both of which result from the general warming of the model atmosphere. For further discussion of this topic, see MW80.

Table 3 contains the area-mean surface air temperature obtained from all the VC experiments conducted in this study. This table reveals that the sensitivity of the VC model climate is reduced with increasing insolation. This reduction partly results from the weakening of the effect of the snow-albedo feedback mechanism with increasing temperature. Ramanathan (1977) pointed out that the "cloud-altitude feedback" mechanism, which is identified in his paper, can be partly responsible for the nonlinearity of the sensitivity of the model climate.

It is of interest that the difference of area-mean surface air temperature between the VC2 and VC4 atmospheres is ~3.2°C which is very similar to the response of the model of WM75 to a 2% increase of the solar constant. This coincidence is reasonable because the surface air temperatures of both the current VC2 experiment and the standard model atmosphere of WM75 are very similar to one another.[2] As pointed out above, the area mean surface air temperature strongly controls the sensitivity of a model climate by determining the area of snowcover.

TABLE 3. The area-mean surface air temperature $\bar{T}_a^A$ for each VC model atmosphere and its deviation $\Delta\bar{T}_a^A$ from the VCS atmosphere.

Experiment	$\bar{T}_a^A$	$\Delta\bar{T}_a^A$
VCS	290.4	0
VC2	294.4	4.0
VC4	297.6	7.2
VC6	299.9	9.5

b. Precipitation

The latitudinal distributions of the rates of precipitation and evaporation from the VCS and VC6 model are illustrated in Fig. 3. This figure clearly indicates that rates of both precipitation and evaporation increase with increasing solar radiation. Poleward of 50° latitude, the increase in precipitation rate is particularly large and is significantly larger than the increase in evaporation rate, which does not vary substantially with respect to latitude. This large increase is responsible for the abundant runoff over the continent in high latitudes of the VC6 model. As discussed in MW80, the large fractional increase in the poleward transport of latent energy in response to the increase in solar radiation is responsible for this result.

Another feature of interest in Fig. 3 is the large fractional decrease in the snowfall rate in response to the increase of the solar constant. Since this subject is extensively discussed in WM75, it is not discussed here.

Table 4 contains the area-mean rates of precipitation from all of the VC experiments. This table indicates that the area-mean precipitation rate increases by as much as 24% in response to a 6% increase of the solar constant. The basic causes for this large fractional increase in the intensity of the hydrologic cycle are discussed in WM75 and are not repeated here.

c. General circulation

Fig. 4 shows the latitude-height distribution of the difference in the zonal wind between the VC6 and VCS atmospheres. In addition, the distribution of the zonal wind itself in the VCS atmosphere is

[2] Note that the VC2 experiment of the present study is used as a standard experiment in the CO_2 sensitivity study of Manabe and Wetherald (1980).

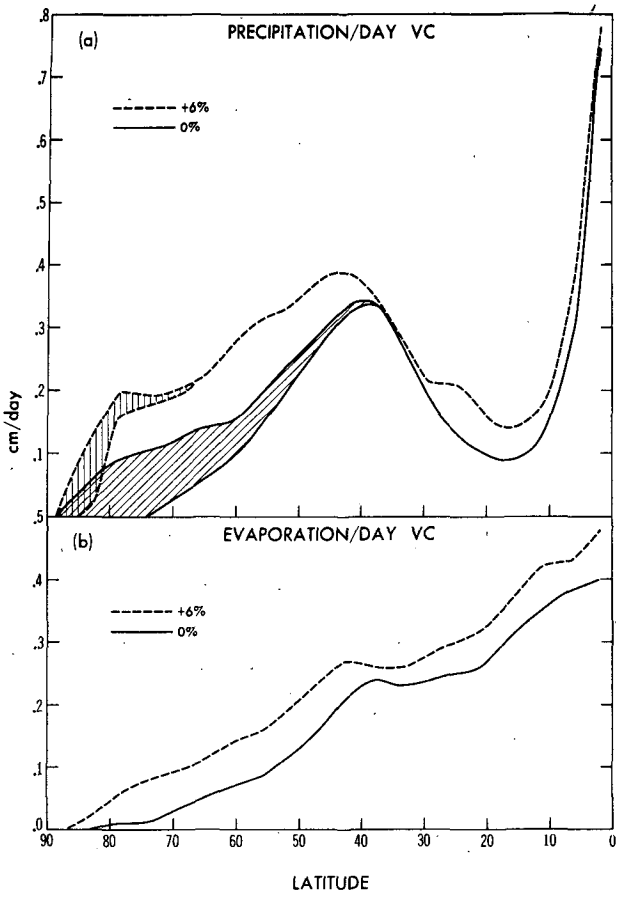

FIG. 3. (a) Zonal-mean rates of total precipitation. Hatched areas denote portion of the precipitation rate attributable to snowfall. (b) Zonal-mean rates of evaporation. Solid and dashed lines indicate the results from the VCS and VC6 experiment, respectively. Units are in cm day^{-1}.

added as a reference. According to this figure, the intensity of the zonal wind is reduced significantly in the latitude belt ranging from 15 to 40° in response to the increase of the solar constant. From the consideration of the thermal wind relationship, it is clear that this reduction results from the relatively large decrease of the meridional temperature gradient in this latitude belt (refer to Fig. 2b).

It is expected that the change in the vertical wind shear, described above, alters the magnitude of eddy kinetic energy in the model atmosphere. Fig. 5 shows the latitude-height distribution of the difference in eddy kinetic energy between the VC6 and VCS atmospheres. According to this figure, eddy kinetic energy significantly decreases in the middle and lower model troposphere but increases above the 300 mb level of the model atmosphere in response to the increase of the solar constant. This tropospheric reduction of eddy kinetic energy is particularly large around 35° latitude where the vertical wind shear decreases the most as Fig. 4 indicates. As suggested by MW75, the increase of eddy kinetic energy above the 300 mb level may result from the reduction of static stability in the upper troposphere and lower stratosphere of the model, which is evident in Fig. 2b. Further study is required to confirm this speculation.

Fig. 6, which shows the streamfunctions of the meridional circulation in both VCS and VC6 atmospheres, indicates that the overall intensity of the meridional circulation diminishes in response to the increase of the solar constant. It is probable that the weakening of the Ferrel cell results from the aforementioned reduction of eddy kinetic energy in middle latitudes. In summary, the general reduction of the meridional temperature gradient discussed earlier may have caused the weakening of not only the direct circulation of the Hadley cell and the polar cell but also the indirect Ferrel cell.

For the convenience of later discussions, it is useful to discuss the change of the variance of the deviation of the vertical p-velocity from its zonal mean which occurs in response to the increase of the solar constant. Fig. 7b illustrates the latitude-height distribution of the difference in the spatial variance of the vertical p-velocity between the VC6 and VCS atmosphere. For reference, the distribution of this variance for the VCS atmosphere is added as Fig. 7a. According to this figure, the variance increases in the middle and upper model troposphere in response to the increase of the solar constant. Fig. 8, showing the latitude-height distribution of the difference in the rate of temperature change due to moist convection, nonconvective condensation, and the vertical subgrid-scale transport of sensible heat, indicates that condensational heating is also enhanced in the upper and middle troposphere of the model. (Note that the temperature change due to the vertical subgrid-scale sensible heat transport is limited to the planetary boundary layer. Thus, the difference in the upper and middle troposphere is essentially due to moist processes.) This correspondence between the two distributions suggests the mutually enhancing relationship between the condensational heating and large-scale vertical motion.

TABLE 4. Area-mean precipitation rates $\bar{p}^A$ (cm day^{-1}) from the VCS experiment and the fractional increases of precipitation rate in response to the increases in solar constant.

Experiment	$\bar{p}^A$	Fractional increase
VCS	0.235	0.00
VC2	0.258	0.10
VC4	0.277	0.18
VC6	0.291	0.24

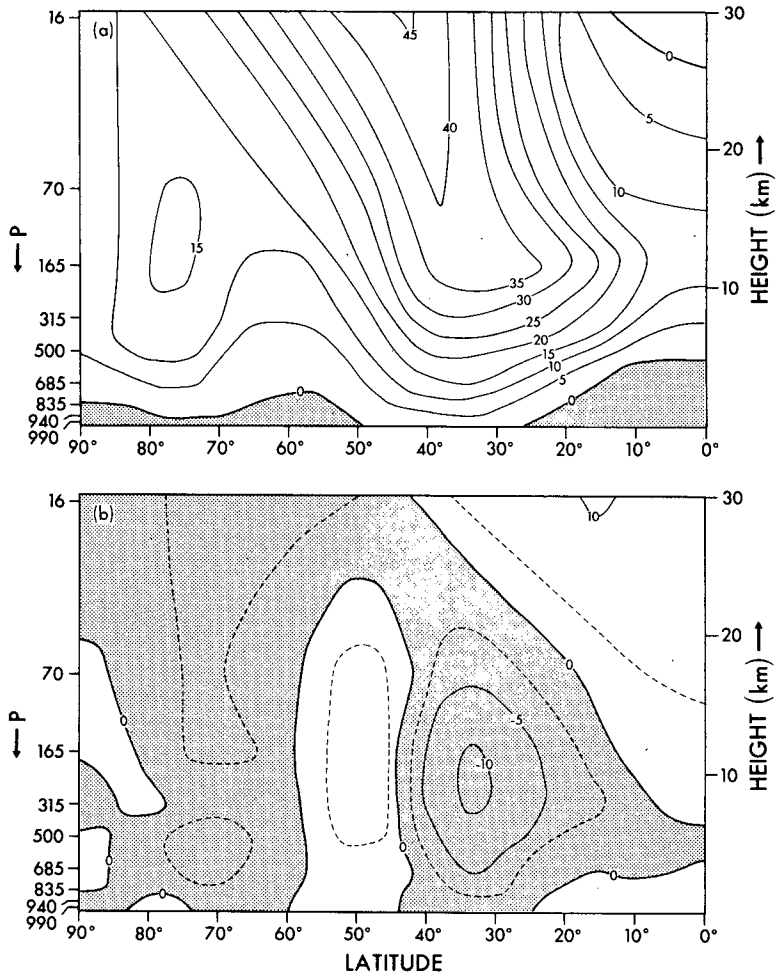

FIG. 4. (a) Latitude-height distribution of zonal-mean wind velocity in the VCS atmosphere. (b) Latitude-height distribution of the difference in zonal-mean wind velocity between the VC6 and VCS atmosphere. Shaded areas denote negative values. Units are in m s^{-1}.

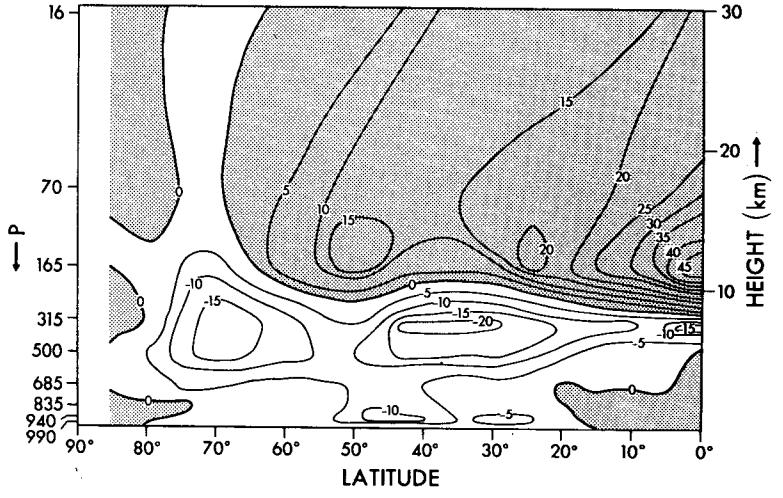

FIG. 5. Latitude-height distribution of the zonal mean difference in eddy kinetic energy between the VC6 and VCS atmosphere. Units are in J kg^{-1} cm^{-2}.

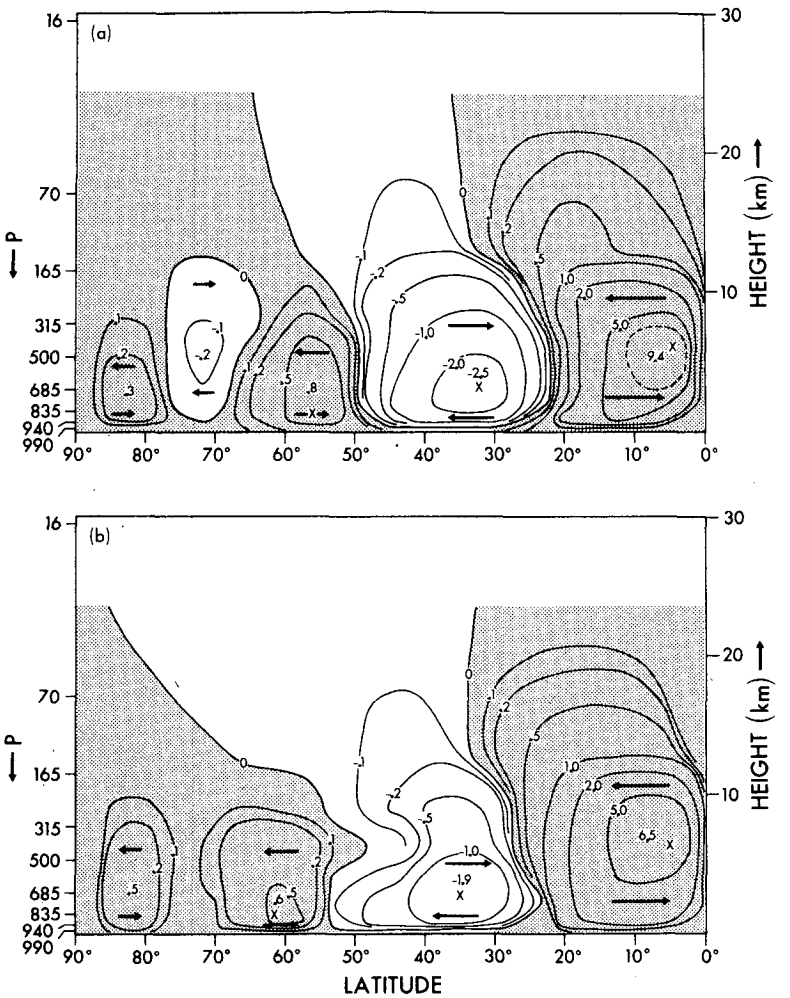

FIG. 6. Latitude-height distributions of the streamfunction units, 10^{13} g s^{-1}. (a) VCS atmosphere. (b) VC6 atmosphere.

d. Cloud cover

1) SIMULATION OF CLOUD COVER

Before discussing how the change in cloud cover affects the response of the model climate to a change of the solar constant, it is desirable to describe the distribution of the cloud cover that is simulated by the VCS model. Fig. 9 shows the latitude-height distribution of the zonal-mean cloud amount from the VCS model. This figure reveals that in the VCS model atmosphere cloud amount is at a minimum in the subtropics where the downward motion branch of the Hadley cell is located. In addition, one can identify a layer of relatively large cloudiness in the upper model troposphere and a thin layer of large cloudiness near the earth's surface in high latitudes. As one might expect, the distribution of cloudiness described above has some resemblance to the distribution of zonal-mean relative humidity, which is shown in Fig. 10.

For further examination, cloud cover is classified in two categories, i.e., convective and non-convective cloud. When the static stability of the cloudy layer is supercritical, it is assumed that the layer contains convective cloud. Otherwise, a cloud is assumed to be nonconvective. Fig. 11 contains the latitude-height distributions of nonconvective and convective cloud amount in the model atmosphere. This figure indicates that in the model atmosphere, convective cloudiness is much smaller than nonconvective cloudiness. It is reasonable that the convective cloudiness of the VCS atmosphere is relatively large in the tropics and around 45° latitude where the rainbelts of the tropics and middle latitudes are located. Out of these convectively active regions which are identified above, nonconvective clouds spread upward and laterally into the upper model troposphere. The heights of these nonconvective cloud layers in the model atmosphere are ~12 km in the tropics, 8 km in middle latitudes,

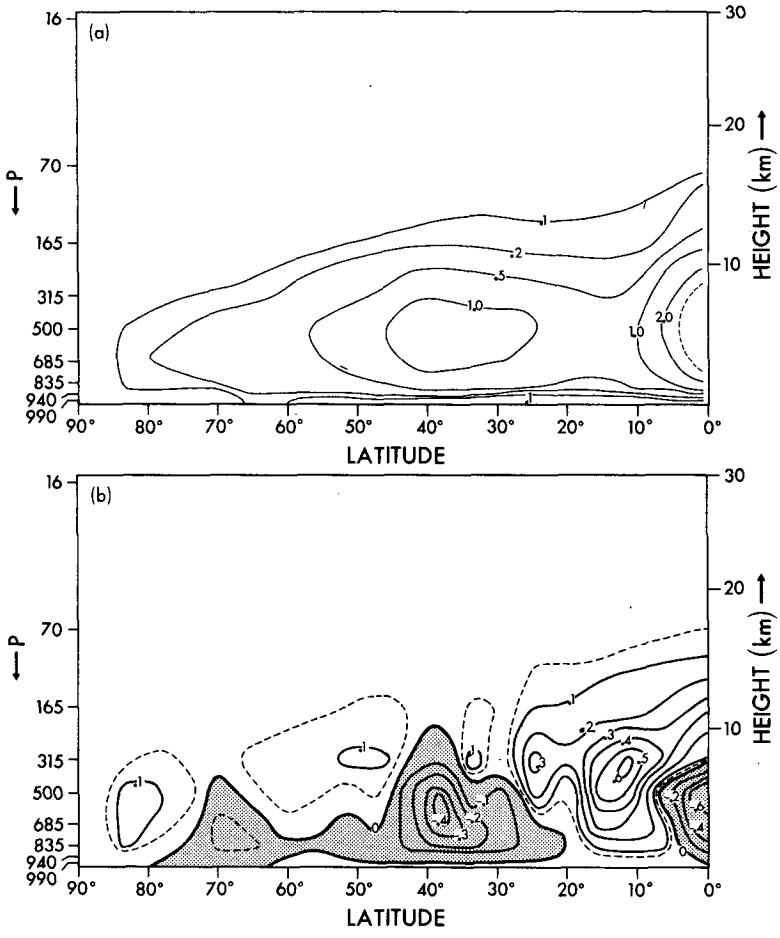

FIG. 7. (a) Latitude-height distribution of the variance of the deviation of vertical p-velocity from its zonal mean in the VCS atmosphere. (b) Latitude-height distribution of the difference in the variance of the deviation of vertical p-velocity from its zonal mean between the VC6 and VCS atmospheres. Units are in dyn^2 cm^{-4} s^{-2}.

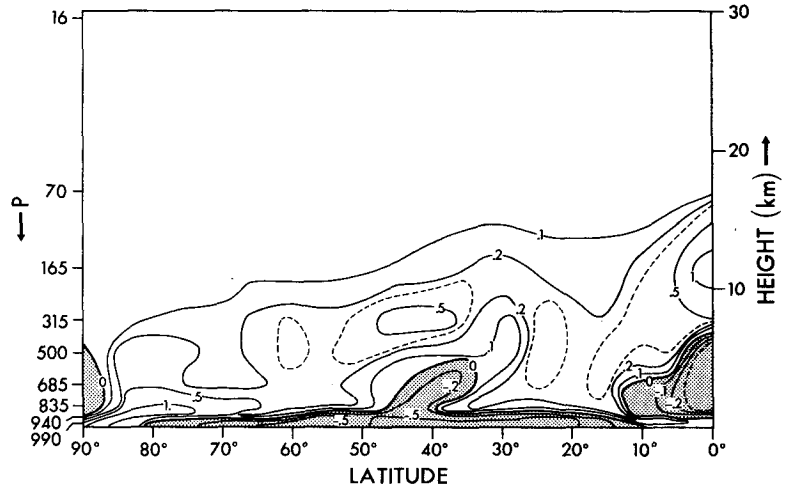

FIG. 8. Latitude-height distribution of the difference (VC6 minus VCS atmosphere) in the rate of the net temperature change due to moist convection, nonconvective condensation and vertical subgrid-scale transport of sensible heat (units, K day^{-1}).

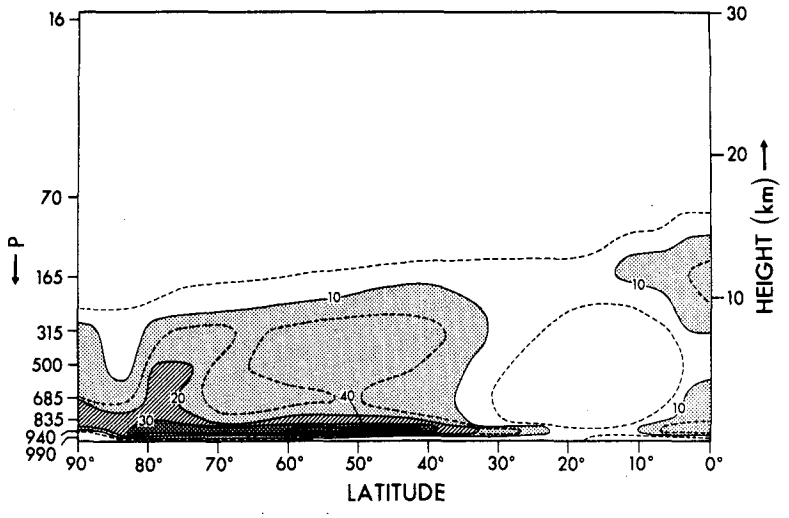

FIG. 9. Latitude-height distribution of zonal-mean cloudiness in the VCS atmosphere. Units are in percent.

and ~6 km in high latitudes. In view of the characteristics described above, it may not be unreasonable to regard these upper tropospheric clouds as cirrus clouds.

In the model subtropics, where relative humidity is low because of the general subsidence of air, the amounts of both convective and nonconvective clouds are significant only in the lowest layer of the model atmosphere, i.e., the planetary boundary layer.

In high latitudes of the model, relative humidity is high and accordingly, nonconvective cloud occupies a large fraction of area near the earth's surface. In this latitude region, moisture from the underlying surface is trapped in the lowest layer of the model atmosphere because of the stable stratification there. Furthermore, net radiative cooling of low cloud is intense owing to strong emission of long wave radiation from the cloud top and the smallness of the absorption of solar radiation. In short, the high level of relative humidity resulting from net radiative cooling and trapping of water vapor near the earth's surface is responsible for sustaining an extensive low cloud layer in high latitudes of the model.

The distribution of zonal-mean cloud described above may be compared with the observed annual-mean cloud distribution constructed from seasonal data compiled by Telegadas and London (1954) and London (1957) and is shown in Fig. 12. According

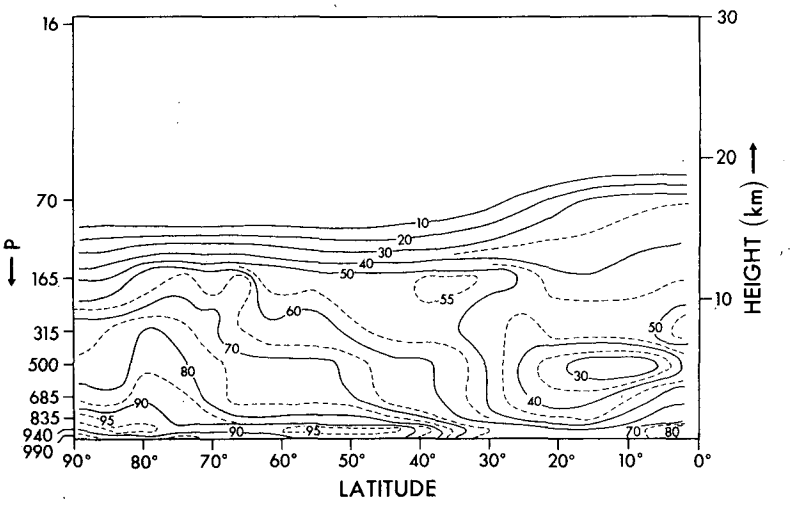

FIG. 10. Latitude-height distribution of zonal-mean relative humidity in the VCS atmosphere. Units are in percent. A convective cloud is located wherever the moist convective adjustment occurs.

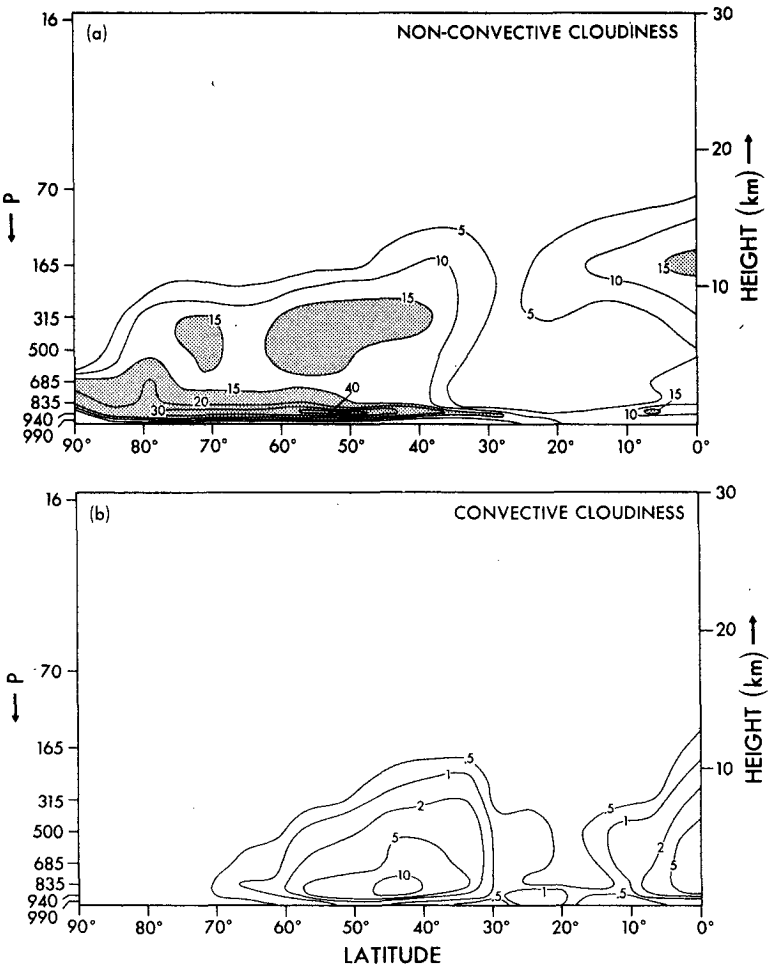

FIG. 11. Latitude-height distribution of non-convective cloudiness (a) and convective cloudiness (b). Units are in percent.

to this comparison, the latitudinal variation of the altitude of maximum cloud amount in the upper model troposphere corresponds reasonably well with the latitude variation in the height of cirrus cloud as determined by London. Furthermore, the extensive layer of low cloud in higher latitudes of the model may be identified with the stratus cloud layer contained in London's distribution, although the computed altitude is somewhat lower than the observed and the amount of low cloud is significantly overestimated by the model. In London's result, one can identify a cloud-free layer beneath the cirrus cloud. The VCS model fails to simulate this cloud gap though the model atmosphere has a region of relatively low cloudiness in the midtroposphere. This region of minimum cloudiness is particularly evident in the simulated distribution of nonconvective cloud. In summary, the distribution of zonal-mean cloud in the model atmosphere resembles reasonably well the observed distributions compiled by London.

In Fig. 13 the distribution of the zonal mean total cloudiness obtained from the VCS-experiment is compared with the observed distributions in both hemispheres. In general, the agreement between the computed and observed cloud amount is fair. One notes that there are large differences among various versions of the observed cloud distributions. Nevertheless, the simulated cloudiness appears to be significantly less than the estimates of the actual cloudiness at most latitudes, particularly in the subtropics.

2) CLOUD RESPONSE

The latitude-height distribution of the difference in zonal-mean cloudiness between the VC6 and VCS atmospheres is shown in Fig. 14. According to this figure, cloud amount generally diminishes in most of the model troposphere in response to the increase of the solar constant with the exception of the layer near the earth's surface. In this layer the amount

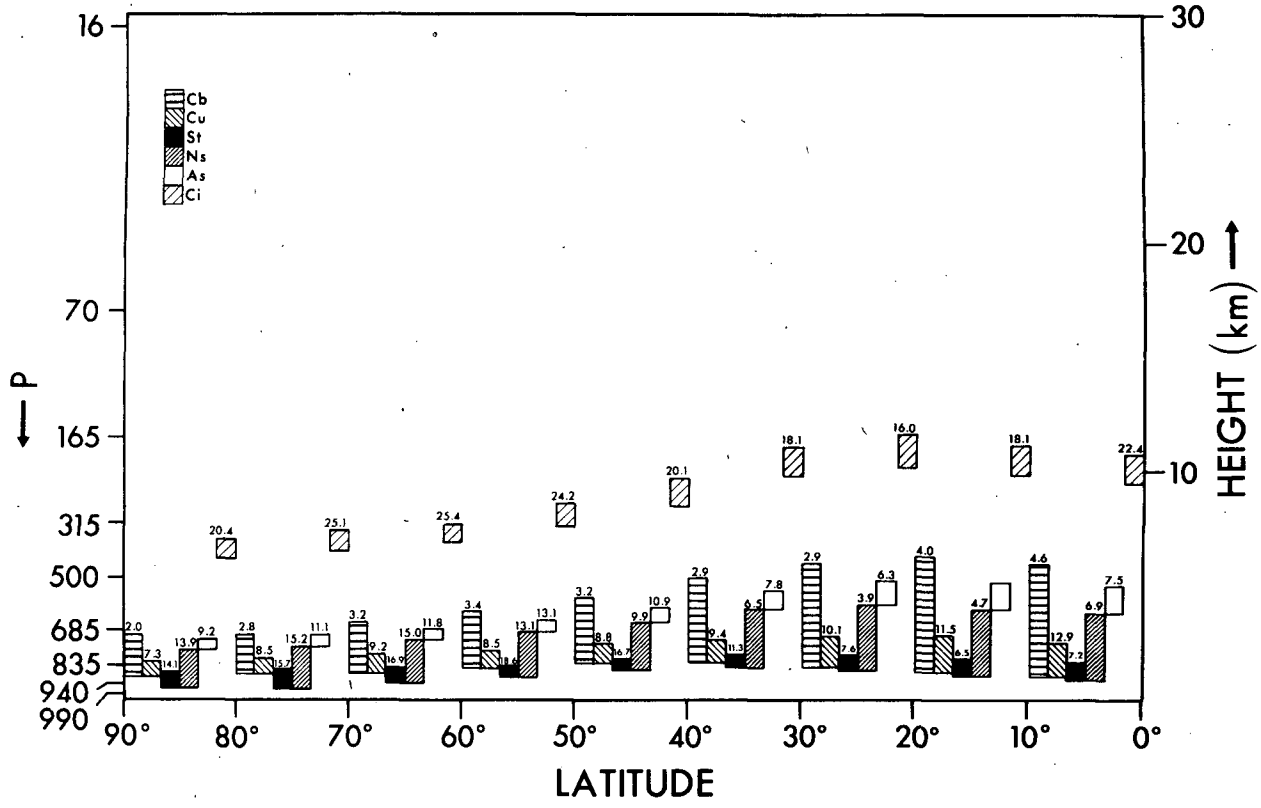

FIG. 12. Diagram depicting the annual-mean cloud distribution computed from the data compiled by London (1957). The different bars show vertical extents of various cloud types, whereas the numbers on top of each bar refer to the cloud amount in percent for that particular cloud type.

of low cloud increases poleward of 50° latitude and in the subtropics but decreases in the tropics and the middle latitudes. In the lower stratosphere of the model, cloud amount tends to increase particularly in high latitudes. Averaged over the entire computational domain, cloud cover increases near the earth's surface and just above the tropopause but decreases in most of the model troposphere, as

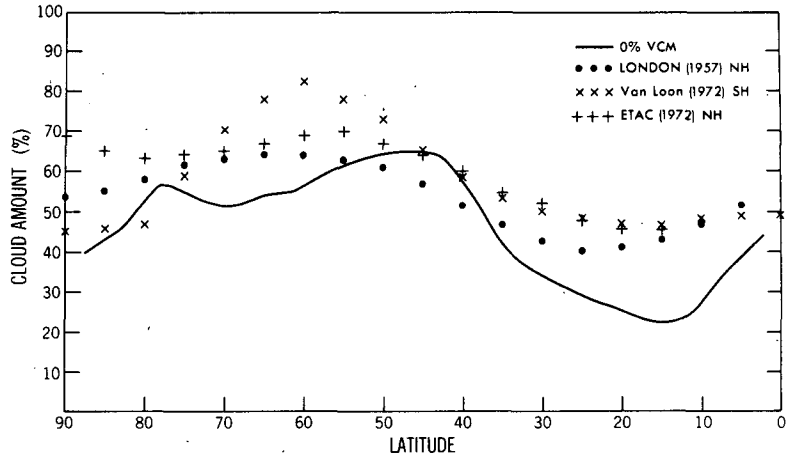

FIG. 13. Latitudinal distribution of zonal-mean total cloudiness in the VCS atmosphere (solid line). The results from the analysis of observed zonal-mean cloudiness in the Northern Hemisphere (London, 1957: ETAC, 1972) and in the Southern Hemisphere (van Loon, 1972) are plotted for comparison. The total cloudiness compiled by ETAC (Environmental Technical Applications Center) is obtained from Schutz and Gates (1973, 1974).

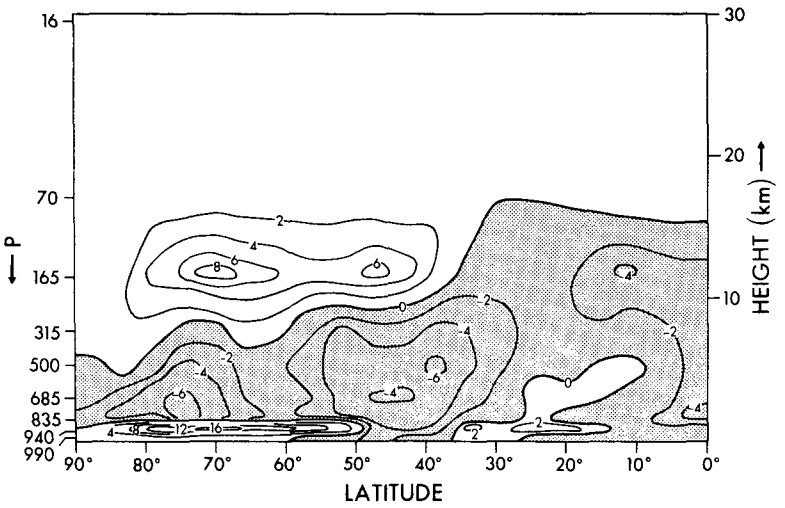

FIG. 14. Latitude-height distribution of the difference in zonal-mean cloud amount between the VC6 and VCS atmosphere. Shaded areas indicate negative values. Units are in percent.

illustrated in Fig. 15. Though there are some exceptions, the change of cloud cover described above resembles qualitatively the change of relative humidity, which is illustrated in Fig. 16.

For example, a comparison between Figs. 14 and 16 reveals that, in high latitudes and the subtropics, both relative humidity and cloud amount increase markedly near the earth's surface in response to the increase of the solar constant. As pointed out in WM75, warming of the earth's surface contributes to the reduction of "Bowen's ratio," i.e., the ratio of sensible heat to latent heat flux into the, at-

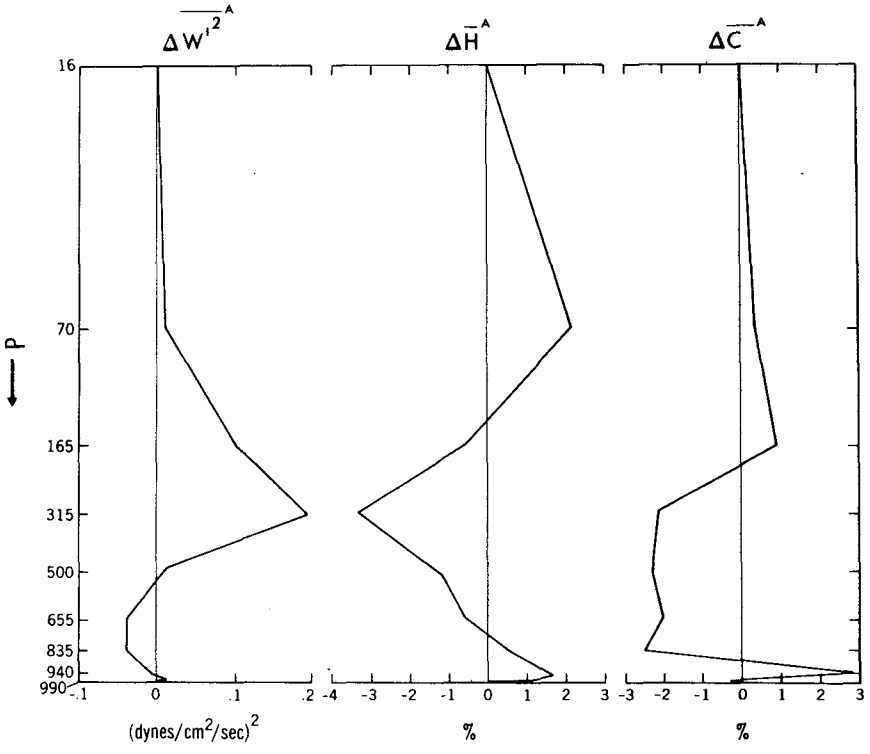

FIG. 15. Vertical distributions of the area-mean differences in the variance of the deviation of vertical p-velocity from zonal mean W' (left), relative humidity H (middle) and cloudiness C (right) between the VC6 and VCS atmosphere.

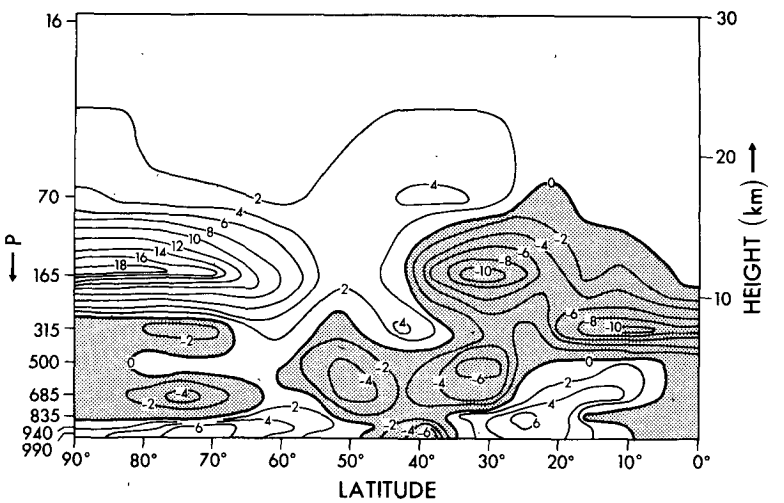

FIG. 16. Latitude-height distribution of the difference in zonal-mean relative humidity between the VC6 and the VCS atmosphere. Units are in percent.

mosphere. A highly nonlinear increase of saturation vapor pressure with increasing surface temperature contributes to the enhancement of evaporation and is responsible for this reduction. Since the warming is at a maximum at the earth's surface and sharply decreases with increasing altitude, it is expected that the enhanced evaporation from the underlying surface contributes to the increase of relative humidity at a level located slightly above the earth's surface. It is also reasonable that the increase of low cloud occurs in high latitudes and the subtropics, where the lowest layer of the model atmosphere has a relatively stable stratification and tends to prevent the penetration of moist air toward higher levels.

In the upper and middle troposphere of the model, both cloud amount and relative humidity decrease significantly at most latitudes in response to the increase of the solar constant. It was suggested in WM75 that this reduction of relative humidity results from the upper tropospheric increase in the variance of vertical p velocity which is caused by the enhanced release of condensation heat (see Section 4b). The intensifications of both downward and upward motion result in the overall increase in precipitation rate and is responsible for the lowering of the area-mean relative humidity. In other words, the drying in the region of subsidence tends to be larger than the moistening in the region of upward motion because the relative humidity cannot exceed 100% due to saturation. Thus the larger the variance of vertical velocity, the less is the area-mean relative humidity. The results of the present experiments shown in Fig. 15 appear to support this conclusion. According to this figure, the reduction of the area-mean relative humidity is at a maximum around the 315 mb level where the increase in the variance of vertical p-velocity is most pronounced.

The general reduction of cloudiness in the middle and the upper model troposphere discussed above is not uniform with respect to latitude. For example, the reduction is relatively large in the equatorial and the middle-latitude belt where the upward motion branches of the meridional circulation are located in the model atmosphere, as Fig. 6a indicates. It is possible that the general weakening of the meridional circulation discussed in Section 4c is responsible for the reduction of both relative humidity and cloudiness in the latitude belts identified above.

So far, only the change of cloudiness in the model troposphere has been described. According to Figs. 14 and 16, both cloudiness and relative humidity increase in the lower model stratosphere, particularly in high latitudes. Fig. 2b shows that the warming of the model troposphere, which occurs in response to the increase of the solar constant, is much larger than the corresponding warming of the model stratosphere. It is expected that the reduction of the static stability around the tropopause level, which results from the aforementioned difference in the temperature change between the stratosphere and the troposphere, enhances the upward moisture transport by large-scale eddies across the tropopause and contributes to the increase of relative humidity in the lower model stratosphere where the warming is relatively small. Therefore, it appears reasonable that the increase in both relative humidity and cloudiness is particularly large in the lower model stratosphere of high latitudes where the reduction of static stability is relatively large, as Fig. 2b indicates. The mechanism for the increase of the lower stratospheric cloud

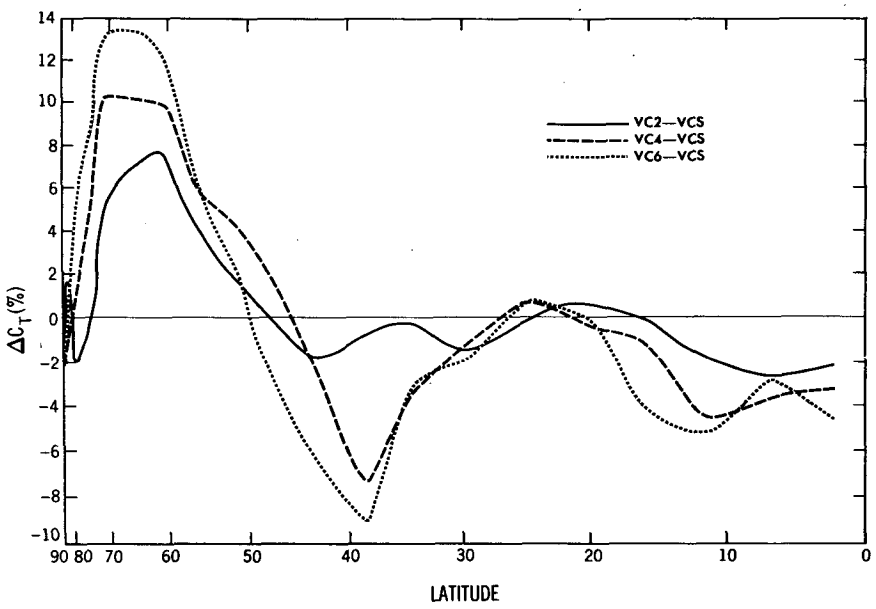

FIG. 17. Latitudinal distribution of zonal mean difference in total cloudiness (%) between a VC and the VCS atmosphere.

described above is very similar to the mechanism for the increase of stratus cloud in the lower model troposphere in high latitudes, discussed earlier.

In the preceding discussion, it is pointed out that an increase (or reduction) in zonal mean relative humidity accompanies the increase (or reduction) of zonal mean cloudiness. However, the former does not necessarily imply the latter. As a matter of fact, a further examination of Figs. 15 and 16 indicates that there are significant differences between the distribution of cloudiness change and that of relative humidity. For example, Fig. 15 reveals that at the 835 mb level, the area-mean cloudiness significantly decreases, whereas the area-mean relative humidity changes little. In order to appreciate this difference, it is necessary to analyze the spatial and temporal variation of vertical velocity and their effect on the fractional coverage of saturated (cloudy) area. Although such an analysis has been made, a satisfactory picture of the relationship among the changes in humidity, vertical velocity and cloudiness has not emerged. This is a topic for future study.

The latitude-height distributions of the zonal-mean change of cloud cover that have been discussed so far amount to the zonal-mean changes of total cloudiness shown in Fig. 17. This figure indicates that, in response to the increase of the solar constant, total cloudiness diminishes equatorward of 50° latitude with the exception of a narrow subtropical belt, whereas it increases significantly poleward of 50° latitude. The reduction of cloud cover in the upper and middle troposphere is responsible for not only the reduction of total cloudiness but also the lowering of the effective cloud top height in lower latitudes. (This is because the magnitude of the area mean change of low cloud amount equatorward of 50° latitude is very small and is less than the reduction of cloud amount in the upper and middle model troposphere, as Fig. 14 indicates. Thus, the changes in the relative magnitude of cloud amount at different altitudes result in the change of the effective cloud-top height.) Poleward of 50° latitude, the increase of cloud amount near the earth's surface and in the lower stratosphere of the model overcomes the reduction of cloudiness in the middle model troposphere and accounts for the substantial increase of total cloudiness.

Because of the compensation between the change of total cloudiness in high latitudes and the change in lower latitudes, the total cloud amount over the entire computational domain changes little in response to the increase of the solar constant. This is evident in Table 5, which tabulates the area-mean value of total cloudiness obtained from all four experiments.

e. Radiative flux

The change in net radiative flux R at the top of the model atmosphere, in response to a 6% increase of the solar constant, is given by

$$\delta R = \delta S - \delta F, \qquad (1)$$

where $\delta(\ )$ denotes the increment $(\ )$ from the VCS to VC6 atmospheres. S and F are net

TABLE 5. The area mean cloudiness (percent) for each VC experiment

Experiment	Cloudiness
VCS	42.6
VC2	42.7
VC4	42.4
VC6	41.9

downward solar radiation and upward terrestrial radiation at the top of the model atmosphere, respectively. S and F are approximated as follows:

$$\delta S \approx \delta_I S + \delta_r S + \delta_C S + \delta_\alpha S, \quad (2)$$

$$\delta F \approx \delta_T F + \delta_r F + \delta_C F. \quad (3)$$

Here, $\delta_x S$ and $\delta_x F$ indicate changes in S and F responding to the change in a quantity x when it is assumed that all other relevant variables are unchanged. Suffixes I, T, r, C and denote solar constant, atmospheric temperature, mixing ratio of water vapor in air, cloud cover and surface albedo (for solar radiation), respectively. From physical considerations, it is obvious that $\delta_I F = \delta_\alpha F = \delta_T S = 0$. Owing to nonlinear dependence of S and F on these factors, the sums of all parts approximately, but not exactly, add up to δS and δF. The following equation, which defines $\delta_C F$, indicates by example the procedure for computing each term in the right-hand side of Eqs. (2) and (3):

$$\delta_C F = F(^\circ I, \{^\circ T_i\}, \{^\circ r_i\}, \{^6 C_i\}, {}^\circ\alpha) - F(^\circ I, \{^\circ T_i\}, \{^\circ r_i\}, \{^\circ C_i\}, {}^\circ\alpha), \quad (4)$$

where superscript $^\circ$ and ^{6} indicate the data from the VCS and the VC6 experiment respectively. $\{T_i\}$, $\{r_i\}$ and $\{C_i\}$ indicate sets of temperature, mixing ratio of water vapor and cloudiness at all finite-difference levels of the model.

Table 6 contains the values of $\overline{\delta_x Y}^A$. This table illustrates how each of the various relevant factors contributes to the changes in radiative fluxes δR, δS and δF. For example, it shows that the change in surface albedo due to the poleward retreat of snowcover has a significant positive contribution to δR, indicating the positive feedback effect of snowcover variation. The table also reveals that the increase of water vapor mixing ratio in air in response to the 6% increase of the solar constant also has a large positive contribution to R, implying the strong positive feedback effect of water vapor variation. On the other hand, the contributions of $\overline{\delta_C S}^A$ and $\overline{\delta_C F}^A$ to $\delta_C R$ almost compensate each other, indicating the smallness of the net contribution of the cloud feedback mechanism on the radiation balance of the atmosphere.

In order to appreciate the specific mechanisms of compensation mentioned above, it is desirable to subdivide the changes of radiative fluxes resulting from the cloudiness change into two parts, i.e.,

$$\delta_C S = \delta_{CA} S + \delta_{CH} S, \quad (5)$$

$$\delta_C F = \delta_{CA} F + \delta_{CH} F, \quad (6)$$

where $\delta_{CA} Y$ and $\delta_{CH} Y$ denote the changes of flux Y due to the change in cloud amount and cloud height, respectively. In these equations, $\delta_{CA} Y$ is defined by the following equation

$$\delta_{CA} Y = \sum_i \frac{\delta Y}{\delta C_i} \delta_A C_i, \quad (7)$$

where $\delta_A C_i \equiv C_i(\delta C_T / C_T)$, and

$$C_T = \prod_i (1 - C_i),$$

C_i denotes cloud amount at the ith finite-difference level and C_T denote total cloudiness. In other words, $\delta_{CA} Y$ denotes the change of Y which occurs when the cloud amounts at all finite-difference levels $\{C_i\}$ change by a constant factor $\delta C_T / C_T$. The remainder of the cloud-induced change in Y is defined as $\delta_{CH} Y$, i.e.,

$$\delta_{CH} Y = \delta_C Y - \delta_{CA} Y. \quad (8)$$

The latitudinal distributions of zonal-mean values of $\delta_{CA} S$, $\delta_{CH} S$, $-\delta_{CA} F$, and $-\delta_{CH} F$ are shown in Fig. 18. Note that the length scale of the abscissas in this figure are proportional to the sine of the latitude so that its increment is proportional to the area of the latitude belt.

In the preceding subsection it is shown that the total cloudiness in the VC model mostly decreases equatorward of 50° latitude and increases poleward of 50° latitude in response to the increase

TABLE 6. Table $\delta_x Y$. $\delta_x Y$ denotes the change of Y (i.e., S, F or R) attributable to the change in X (i.e., s, T, r, C or α). The $\sum$ column represents the sum of all relevant $\delta_x Y$. See the explanations of Eqs. (1), (2) and (3) for further information.

	$\delta_x Y$						
Y	$X = s$	T	r	C	α	$\sum$	δY
S	15.49	—	1.88	2.26	4.74	24.37	24.28
$-F$	—	−32.09	10.19	−2.77	—	−24.67	−24.28
R	15.49	−32.09	12.07	−.51	4.74	−.30	0

of the solar constant. Therefore, the signs of $\delta_C S$ and $\delta_C F$ shown in Fig. 18 reverse themselves around this latitude. However, the area-integrals of the changes $\delta_C S$ and $\delta_C F$ over the high-latitude region are much less than those of the changes in the lower latitudes owing mainly to the smallness of the area of the region.

Equatorward of 50° latitude, the net incoming solar flux increases, because the reduction of cloud amount described in the preceding subsection causes the reduction in reflected solar radiation. In other words, the change in cloudiness significantly increases the solar radiation absorbed by the earth-atmosphere system of the model. On the other hand, the reduction of both amount and effective height of cloud cover in middle and low latitudes increases the outgoing terrestrial radiation at the top of the model atmosphere and contributes to the energy loss from the earth-atmosphere system of the model. Thus, the cloud-induced changes in solar and terrestrial fluxes, described above, compensate each other and make a rather small contribution to the change in the area-mean net radiation flux R.

In high latitudes the increase in cloudiness contributes to the reductions of net incoming solar radiation and the outgoing terrestrial radiation. Both of the reductions tend to compensate each other.

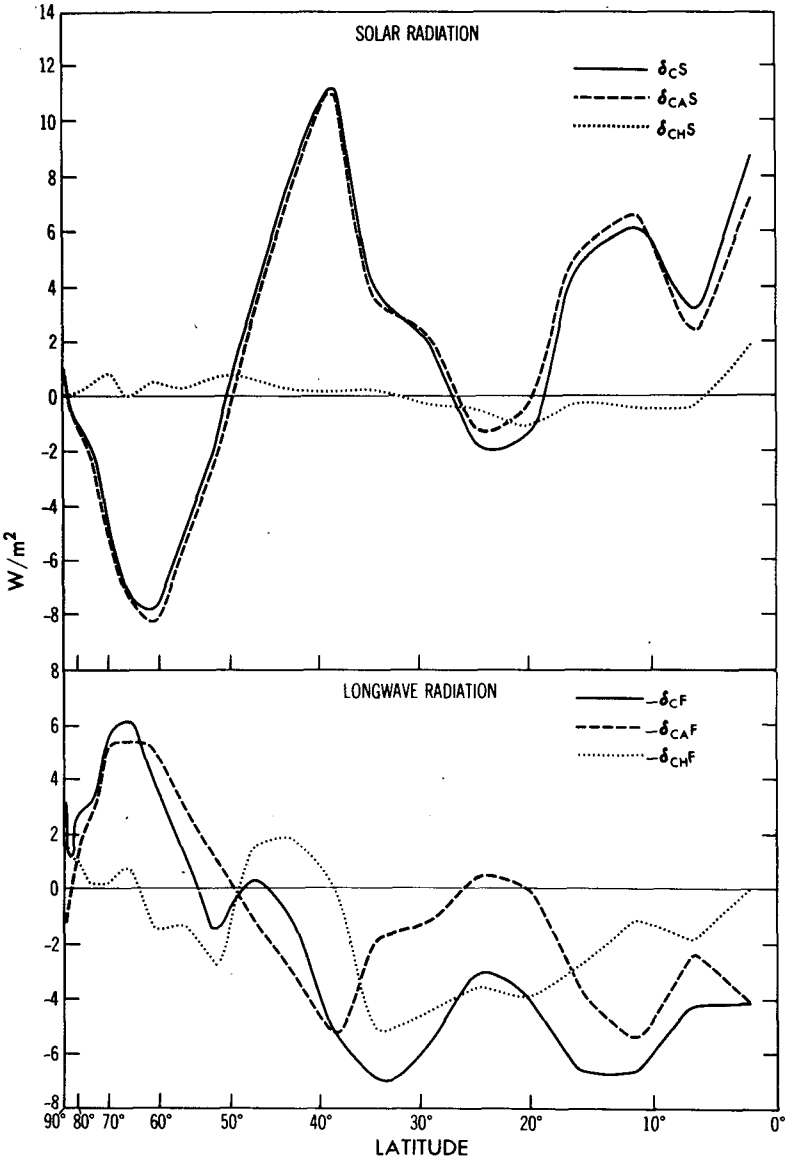

FIG. 18. Upper half: latitudinal distributions of $\delta_C S$, $\delta_{CA} S$ and $\delta_{CH} S$. Lower half: latitudinal distribution of $-\delta_C F$, $-\delta_{CA} F$ and $-\delta_{CH} F$. Units are in W m^{-2}.

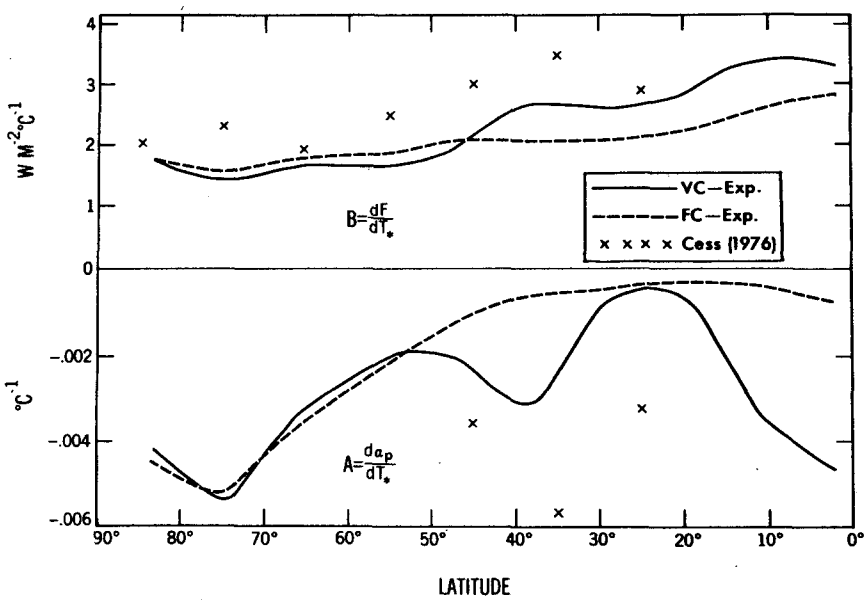

FIG. 19. Latitudinal distributions of A- and B-values obtained by comparing the VC6, VCS and the FC6 and FCS experiments. In addition, the values of A and B obtained by Cess (1976) from satellite observation are indicated by crosses. Top half: A-values in units of W m^{-2} °C^{-1}. Bottom half: B-values in units of °C^{-1}.

Although the effective cloud height hardly changes in these latitudes, the degree of compensation is reasonably good because of the small insolation there.

Owing to the compensation described above, the change of area-mean net radiative flux R resulting from the change in cloudiness is very small, as Table 6 indicates. Therefore, the cloud feedback mechanism has a relatively small influence on the sensitivity of the area-mean model climate, as illustrated in the following section.

However, in view of the uncertainty in the values of the optical parameters of clouds, it is desirable to examine the dependence of the results upon the choice of these parameters before accepting some of the conclusions discussed above. As a matter of fact, some of the values of the optical parameters chosen for this study do not appear to be the most reasonable choice in the light of observational evidence. For example, it is assumed in this study that thin cloud behaves as a blackbody for terrestrial radiation irrespective of its altitude. However, the results of aircraft measurements by Kuhn and Weickmann (1969) indicate that the emissivity of cirrus cloud is significantly less than one. Furthermore, this study assumes that a thin cloud has an albedo of a typical cirrus cloud (i.e., ~20%) when it is located above the altitude of ~10 km. However, the study of Telegadas and London (1954) suggests that a cirrus cloud can exist at a lower altitude (see Fig. 12). Therefore, the changes of radiative fluxes attributable to the change of cloud cover are recomputed on the assumption that a thin cloud located above the altitude of 6 km is half black for terrestrial radiation and has a more typical cirrus albedo. The distributions of temperature, moisture and other parameters required for the computation of radiative transfer are kept unchanged. Table 7 indicates that the degree of compensation between $\overline{\delta_C S}^A$ and $\overline{\delta_C F}^A$, obtained from this cirrus test, is more complete than the compensation obtained from the original VC experiments.

Although the albedos of both thick cloud and low cloud are assumed to be ~50% in this study, other investigators (London, 1957; Rodgers, 1967) chose somewhat larger values. Therefore, the values

TABLE 7. $\overline{\delta_{CA}S}^A$, $\overline{\delta_{CH}S}^A$, $\overline{\delta_C S}^A$, $\overline{\delta_{CA}F}^A$, $\overline{\delta_{CH}F}^A$, $\overline{\delta_C F}^A$, $\overline{\delta_{CA}R}^A$, $\overline{\delta_{CH}R}^A$, $\overline{\delta_C R}^A$ from the VC experiments cirrus test, low cloud test and zenith angle test. $\delta_{CA}(S,F,R)$ and $\delta_{CH}(S,F,R)$ are the changes of (S,F,R) attributable to the changes of amount and height of cloud, respectively. $\delta_C(S,F,R)$ is the sum of $\delta_{CA}(S,F,R)$ and $\delta_{CH}(S,F,R)$. $(\overline{\ })^A$ denotes the area mean. For further explanation, see the main text.

	VC exp.	Cirrus test	Low cloud test	Zenith angle test
$\overline{\delta_{CA}S}^A$	−2.24	2.38	2.80	1.71
$\overline{\delta_{CH}S}^A$	0.02	−0.45	−0.39	0.31
$\overline{\delta_C S}^A$	2.26	1.93	2.41	2.02
$\overline{\delta_{CA}F}^A$	1.14	0.74	1.14	1.14
$\overline{\delta_{CH}F}^A$	1.63	1.23	1.63	1.63
$\overline{\delta_C F}^A$	2.77	1.97	2.77	2.77
$\overline{\delta_{CA}R}^A$	1.09	1.65	1.65	0.57
$\overline{\delta_{CH}R}^A$	−1.60	−1.68	−2.01	−1.32
$\overline{\delta_C R}^A$	−0.51	−0.03	−0.36	−0.75

of $\overline{\delta_C S}^A$ and $\overline{\delta_C F}^A$ are recomputed on the assumption that the albedos of both low cloud and thick cloud are 70%. Again, Table 7 indicates that the $\overline{\delta_C S}^A$ and $\overline{\delta_C F}^A$ from this low cloud test closely compensate each other.

It has been known that the albedo of cloud cover depends significantly on the zenith angle of the sun. Recently, Cess (1976) estimated the zenith angle dependence of cloud albedo from the satellite observations of the seasonal variation in the reflected flux of solar radiation. Based upon the Cess' relationship, which is shown in Fig. 1 of his paper, $\overline{\delta_C S}^A$ and $\overline{\delta_C F}^A$ are reevaluated. As Table 7 indicates, the compensation between $\overline{\delta_C S}^A$ and $\overline{\delta_C F}^A$ obtained from this zenith angle test is not as complete as the compensation obtained from the preceding two tests but is slightly larger than that from the basic VC experiments.

To evaluate satisfactorily the influences of the various parameter changes upon the sensitivity of the model climate, it is desirable to repeat several sets of long-term integrations of the model (i.e., sensitivity experiments) using the revised sets of cloud parameters. This was not done because of the excessive requirement of computer time. Nevertheless, the results from these parameter tests suggest that the compensating relationship described in this section may have a general validity.

It is desirable to assess the validity of the present results in the actual atmosphere by examining whether the actual distributions of cloud cover and radiative fluxes change in a similar manner in response to the change in solar radiation. One example of observable changes of this kind is the seasonal variation of solar radiation, although the fractional change in solar radiation is not constant at all latitudes. Recently, Cess (1976) analyzed the seasonal variations of the fluxes of solar and terrestrial radiation and investigated the dependence of these fluxes on the temperature of the earth's surface. Using the data from satellite observations, he computed two parameters A and B which are defined by the following equations

$$B = \frac{dF}{dT_*}, \quad A = \frac{d\alpha_p}{dT_*},$$

where T_* is the temperature of the earth's surface and α_P is planetary albedo. Budyko (1969) noted that both of these parameters strongly control the sensitivity of climate based on the results from his one-dimensional energy balance model of the atmosphere. However, both Cess (1976) and Budyko (1977) suggested that these parameters are significantly affected by cloud-cover change occurring in response to the change of surface temperature but that the net effect of cloud-cover variation on the sensitivity of climate is relatively small.

Fig. 19 compares the values of A and B obtained from the VC and FC experiments. The difference between the results from these two experiments should reveal the influence of cloud cover variation upon the parameters A and B. In addition, the values of A and B from the observational studies of Cess[3] are plotted in the same figure for comparison. These B-values from the Cess' study are larger than the values of B (i.e., 1.45) obtainable from the earlier study of Budyko (1969). On the other hand, the A values from Cess' study have larger negative values than Budyko's A for an ice-free surface.

According to Fig. 19, B values from the VC experiments are larger than the B values from the FC experiments equatorward of 50° latitude where both cloud amount and effective cloud-top height reduce in response to an increase of solar radiation. These results indicate that the change of cloud cover described above contributes to the increase of the B value in lower latitudes. Although the B values from the observational study of Cess are larger than the B values from the VC experiments as well as those from the FC experiment, the present results suggest that the cloud-cover change partly accounts for the large observational values of B equatorward of 50° latitude.

It is reasonable that the latitudinal distributions of A from both VC and FC experiments indicate a large negative value in high latitudes. The poleward retreat of highly reflective snowcover, which occurs in response to the increase of surface temperature, accounts for this result. In lower latitudes, the magnitude of negative A from the VC experiment is significantly larger than that from the FC experiment. From the earlier discussion of Fig. 18, it is clear that this difference results from the reduction of cloud amount which occurs in the VC atmosphere in response to an increase in the solar constant. Fig. 19 also reveals that the parameter A from Cess' study has a significant negative value in lower latitudes in qualitative agreement with the results from the VC experiment. In short, it is probable that in lower latitudes, the parameter A has a significant negative value partly because of the cloud-cover feedback mechanism.

However, there is a significant difference between the Cess' and the present results. According to Cess' analysis, the cloud-induced modifications of infrared and solar fluxes at the top of the atmosphere almost exactly cancel with each other at each latitude, whereas they do not in the present result. However, they compensate with each other when the changes of these fluxes from the present

[3] The values of B from the Cess study were reevaluated and updated by Warren and Schneider (1979) and proved to be only slightly smaller than those given by Cess (1976).

TABLE 8. Comparison between the area mean surface air temperatures of the model atmospheres from the FC and VC experiments. T_a is the surface air temperature of a model atmosphere and $\Delta\bar{T}_a^A$ is its deviation from the standard atmosphere.

Experiments	$\bar{T}_a^A$	$\Delta\bar{T}_a^A$
FCS	291.9	0
FC2	296.0	4.1
FC4	298.9	7.0
FC6	301.2	9.3
VCS	290.4	0
VC2	294.4	4.0
VC4	297.6	7.2
VC6	299.9	9.5

experiments are averaged over a wide latitude belt ranging from the equator to 50° latitude.

The results described above appear to suggest that it is necessary to consider the cloud-cover variation in order to appreciate the observed values of A and B. It is well known that the increase in B reduces the sensitivity of Budyko's model, whereas a larger value of negative A implies a more sensitive model climate (see, e.g., Cess, 1976). Therefore, cloud-induced modifications of these two parameters in middle and low latitudes of the model tend to have opposing influences upon the sensitivity of the climate of Budyko's model. In conclusion, it is encouraging that the results from the present numerical experiments appear to be consistent with Cess' results though the quantitative aspect of the agreement is far from satisfactory.

5. Differences in sensitivity

In this section, the response of the VC model to the increase in insolation is compared with the corresponding response of the FC model in order to evaluate the influence of the cloud feedback mechanism on the sensitivity of climate.

a. Temperature

Table 8 tabulates the area mean surface temperature from both the FC and VC experiments. In addition, the area mean warmings of the surface air temperature of the VC atmosphere in response to various increases of the solar constant are compared with the corresponding set of temperature changes of the FC model. This comparison reveals that the magnitude of the warming differs little between the VC and FC models.

Table 8 also indicates that the sensitivities of both FC and VC atmospheres decrease with increasing surface air temperature. This is because the increase of surface air temperature results in the reduction of the snowcovered area and, accordingly, the reduction of the influence of the snow-albedo feedback processes on the sensitivity of the model climate. Since the area mean surface air temperatures of the FC atmospheres are slightly warmer than those of the VC atmospheres with the same solar constants, it is premature to conclude (based on the inspection of the last column of Table 8) that the sensitivities of both model atmospheres are identical with each other. For a more proper comparison of the sensitivities, the results of Table 8 are illustrated in Fig. 20 after some processing of the data. On the abscissa of this figure, the solar constants of the FC experiments are normalized by the solar constant used for the standard experiments, whereas those of the VC experiments are normalized by a slightly different value. This value of the solar constant (for normalization) is determined in such a way that it yields the area mean surface air temperature of a VC atmosphere at 291.9 K which is equal to the corresponding temperature of the FCS atmosphere. (The value is estimated by interpolating the solar constants in Table 8.) Thus, one can compare the sensitivities of the FC and VC atmospheres at comparable temperatures. According to this comparison, the sensitivity of the FC atmosphere is slightly larger than that of the VC atmosphere, implying that the cloud feedback process contributes to the slight reduction of the sensitivity of the model climate. This is consistent with the radiation balance analysis of the preceding section where $\delta_C R$ is shown to have

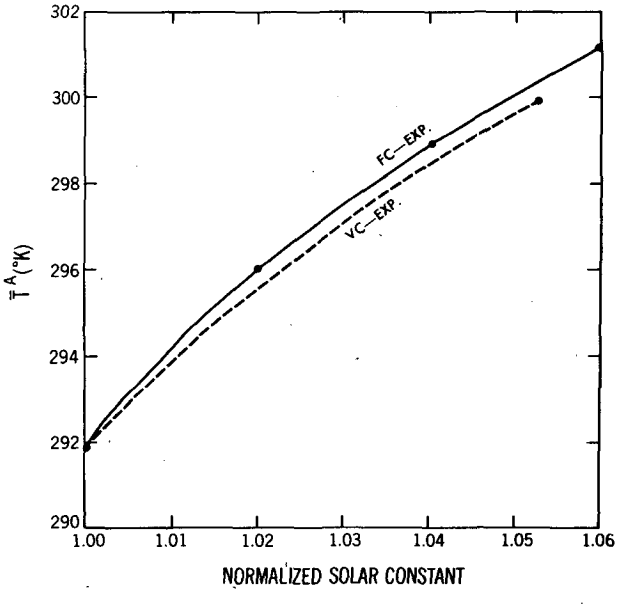

FIG. 20. Relationship between the area mean surface air temperature of the model atmospheres (ordinate) and the normalized solar constant (abscissa). For the FC experiments, the solar constant is normalized by the value of the solar constant used for the FCS experiment. For the VC experiments, it is normalized by the value which yields the area mean surface temperature of 291.9 K for the VC atmosphere. (See the main text for further explanation of this normalization.)

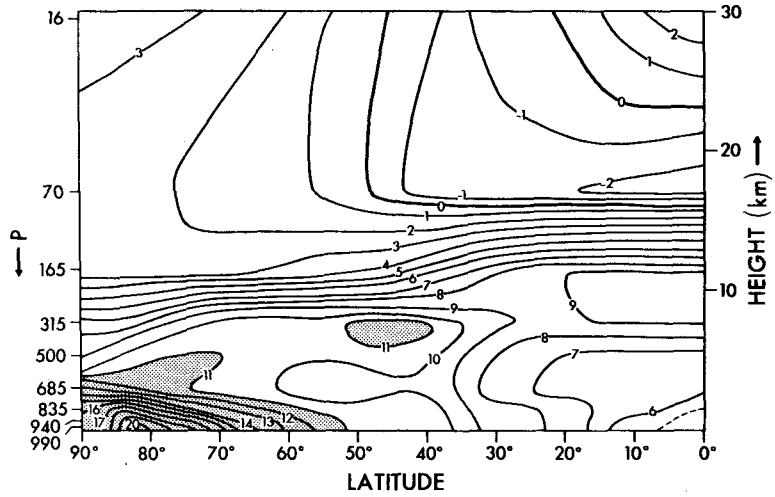

FIG. 21. Latitude-height distribution of the difference in zonal-mean temperature between the FC6 and FCS atmosphere. Units are in K.

a small negative value (see Table 6). Nevertheless, the results from this analysis confirm the preliminary impression from Table 8 that the contribution of the cloud feedback process on the sensitivity of the model climate is small.

Fig. 21 illustrates the latitude-height distribution of the zonal mean difference in temperature between the FC6 and FCS atmospheres. According to the comparison between this figure and Fig. 2b, which shows the similar distribution from the VC experiments, the changes of zonal mean temperature in response to the 6% increase of the solar constant differ little between the FC and VC experiment over most of the model troposphere. (For example, both figures indicate a surface air temperature increase of ~5–6° in the tropics, 10–11° in middle latitudes, and 19–20° in the subpolar region). However, the changes around the tropopause level are significantly different from one another. As Figs. 2b and 21 indicate, the magnitude of the temperature change in the model stratosphere is significantly smaller than the change in the model troposphere for both the VC and FC experiments. However, the variation in magnitude of the change from the troposphere to the stratosphere in the VC experiments is more gradual than the corresponding variation in the FC experiments owing to the difference in cloudiness between the VC6 and VCS experiment.

It is of interest that the areas of negative temperature change appear in the model stratosphere from both the VC and FC experiments. Although a similar feature was found in WM75 (Fig. 3b), it is not known whether this is a statistically significant difference or merely an indicator of the smallness of the temperature response in this region to increases of insolation.

b. Relative humidity

One can examine how the cloud feedback mechanism affects the sensitivity of the humidity field by comparing Fig. 16 and Fig. 22, which show the latitude-height distributions of relative humidity change in response to the 6% increase in the solar constant for the FC and the VC experiments, respectively. In general, the same pattern of relative humidity difference appears to prevail for both sets of experiments, viz., 1) an increase of relative humidity near the earth's surface, particularly in high latitudes; 2) a reduction of relative humidity in the upper and middle troposphere of the model; and 3) an increase of relative humidity in the lower model stratosphere, particularly in high latitudes. Qualitatively, the same results were obtained in WM75 (Fig. 6b).

c. Intensity of the hydrologic cycle

According to Table 9, the fractional increase in the area-mean rate of precipitation in response to a 6% increase of the solar constant is ~24% for both the VC and the FC model. In addition, it was found that changes in latitudinal distributions of rate of precipitation and evaporation in response to 6% increase of the solar constant are very similar between the VC and the FC experiments though some difference exists in the model subtropics.

6. Summary and conclusions

Two series of numerical experiments conducted with the assumptions of either fixed or variable cloud cover suggest that, for the cloud parameterizations used here, cloud feedback mechanisms have

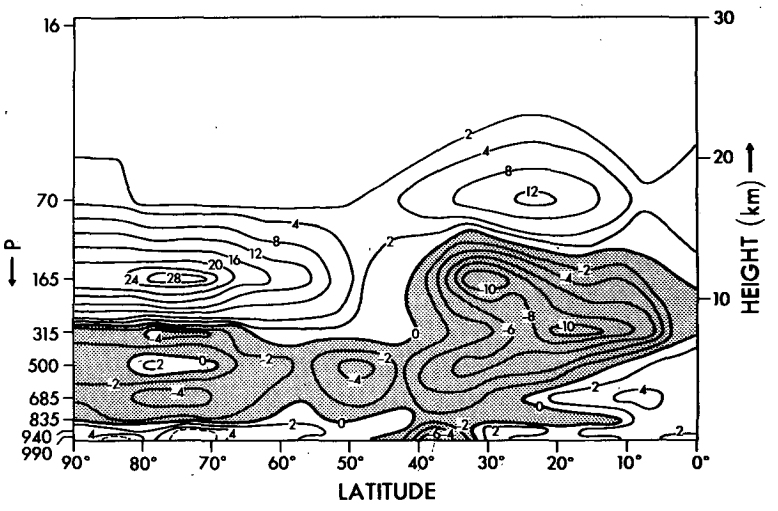

FIG. 22. Latitude-height distribution of the difference in relative humidity between the FC6 and FCS atmospheres. Units are in percent.

a relatively small effect on the sensitivity of area-mean and zonal mean model climate despite a strong influence of cloud cover on solar and terrestrial radiation. Therefore, an extensive analysis of the results from these experiments is performed so that one may determine the mechanisms responsible for this model behavior.

The results from this analysis indicate that the following changes in cloudiness occur in the model atmosphere in response to an increase of the solar constant. In the upper and middle troposphere of the model, both zonal-mean relative humidity and cloudiness decrease because of the increase in the variance of vertical velocity. Owing to the condensation process, the drying in the region of subsidence tends to be larger than the moistening in the region of upward motion. Thus, the reduction of area-mean relative humidity occurs in the layer of intensified vertical velocity. In high latitudes and the subtropics where the atmospheric static stability in the planetary boundary layer of the atmosphere is relatively stable, enhanced evaporation from the warmer surface contributes to the increases in both relative humidity and nonconvective cloudiness at the near-surface level where the warming is less than the surface warming. In the lower stratosphere of the model, nonconvective cloudiness increases particularly in high latitudes. It is suggested that the large reduction in static stability around the tropopause level, which results from the large difference in warming between the troposphere and stratosphere, enhances the upward moisture transport across the tropopause and raises both the relative humidity and cloudiness in the lower stratosphere where the warming is relatively small. In summary, cloudiness decreases in the upper and middle troposphere of the model at most latitudes but increases near the earth's surface and lower model stratosphere mainly in high latitudes in response to an increase of the solar constant.

Because of the change described above, total cloud amount diminishes in most of the region equatorward of 50° latitude, with the exception of a narrow subtropical belt. However, it increases in the region poleward of this latitude. Thus, the net change in the area-mean total cloudiness turns out to be very small. It is found that in both regions the cloud-induced changes in net incoming solar radiation and upward terrestrial radiation at the top of the atmosphere tend to compensate each other. For example, equatorward of 50° latitude, the reductions of cloud amount and effective cloud-top height contribute to the increase in the effective emission temperature of the upward terrestrial radiation and enhance the cooling of the model atmosphere. On the other hand, the aforementioned reduction of cloud amount results in a decrease in reflected solar radiation (or increase in net incoming solar radiation) and thus increases the absorption of incoming solar radiation and con-

TABLE 9. Fractional increase of precipitation rate (relative to a standard experiment).

Experiments	Fractional increase
FCS	0.00
FC2	0.09
FC4	0.16
FC6	0.24
VCS	0.00
VC2	0.10
VC4	0.18
VC6	0.24

tributes to the warming of the earth-atmosphere system of the model.

Poleward of 50° latitude, the increase of total cloud amount contributes to the reductions of both net incoming solar radiation and outgoing terrestrial radiation. Although the effective height of cloud top does not change as it does in lower latitudes, the changes of these two fluxes approximately compensate one another because of the small insolation in high latitudes.

Owing to the compensation mechanism described above, the cloud feedback mechanism has a relatively small effect on the sensitivity of the area-mean climate to a change in solar radiation. This result appears to be in qualitative agreement with the recent suggestions of Budyko (1977) and Cess (1976). A similar result is also obtained from the recent study of Manabe and Wetherald (1980). Using a model identical to the present one, they investigated the sensitivity of climate to an increase in CO_2 concentration in the atmosphere. They noted that the CO_2-induced change of the model climate is hardly affected by the cloud-feedback mechanism. It was found that the distribution of the change of cloud cover is almost identical to that obtained from the present study (refer to Fig. 22 of their study).

In assessing the relevance of the present results to the sensitivity of the actual climate, it is very important to recognize that the method of cloud prediction used for this study is highly idealized. Furthermore, the optical properties of the cloud assumed for the model may not be sufficiently realistic. Therefore, quantitative details of the present result should be regarded with caution.

It is encouraging, however, that a recent numerical time integration of a global model of the atmosphere with realistic geography and sea surface temperature successfully reproduces many of the features of the global distributions of cloud cover and solar and terrestrial radiation obtained from satellite observations. The global model used in this simulation employs a cloud parameterization which is essentially similar to that used in the present study. These results will be presented in a future publication.

In conclusion, the influence of the cloud-feedback mechanism on the sensitivity of the global-mean climate may not be as large as originally suspected because of the compensation-mechanisms identified in this study.

Acknowledgments. The authors would like to express their appreciation to Joseph Smagorinsky, the Director of the Geophysical Fluid Dynamics Laboratory, for his strong support of this sensitivity study. Thanks are also due to Isaac Held and Jerry Mahlman of the Geophysical Fluid Dynamics Laboratory and to V. Ramanathan and Stephen Schneider of the National Center for Atmospheric Research, who gave valuable comments on the preliminary version of the manuscript. Finally, the authors acknowledge Philip Tunison, William Ellis, Michael Zadworney, John Connor and Joyce Kennedy, staff members of the Geophysical Fluid Dynamics Laboratory, who assisted in the preparation of the manuscript.

REFERENCES

Bryan, K., 1966: A scheme for numerical integration of the equations of motion on an irregular grid free of nonlinear instability. *Mon. Wea. Rev.*, **94**, 39–40.

Budyko, M. I., 1958: *The Heat Balance of the Earth's Surface*. Office of Climatology, U.S. Weather Bureau, 255 pp. (Russian translation) [NTIS PB 131692].

——, 1969: The effect of solar radiation variation on the climate of the earth. *Tellus*, **21**, 611–619.

——, 1977: On present-day climate changes. *Tellus*, **29**, 193–204.

Cess, R. D., 1976: Climate change: An appraisal of atmospheric feedback mechanisms employing zonal climatology. *J. Atmos. Sci.*, **33**, 1831–1843.

Drummond, A. J., and J. R. Hickey, 1971: Large-scale reflection and absorption of solar radiation by clouds as influencing earth radiation budgets: New aircraft measurements. *Preprints Int. Conf. Weather Modification*, Canberra, Amer. Meteor. Soc., 267–276.

Held, I. M., and M. J. Suarez, 1974: Simple albedo feedback models of the icecaps. *Tellus*, **26**, 613–629.

Hering, W. S., and T. R. Borden, Jr., 1965: Mean distributions of ozone density over North America, 1963–1964. Rep. No. AFCRL-ERP-162, Air Force Cambridge Research Labs, Mass., 19 pp. [NTIS AD-629 989].

Kuhn, P. M., and H. J. Weickmann, 1969: High altitude radiometric measurements of cirrus. *J. Appl. Meteor.*, **8**, 147–154.

London, J., 1957: A study of the atmospheric heat balance. Final Report, AFCRC Contract AF 19(122)-165, New York University, 99 pp. [DDC AD 117227].

Manabe, S., 1969: Climate and the ocean circulation: I. The atmospheric circulation and the hydrology of the earth's surface. *Mon. Wea. Rev.*, **97**, 739–774.

——, and R. F. Strickler, 1964: Thermal equilibrium of the atmosphere with a convective adjustment. *J. Atmos. Sci.*, **21**, 361–385.

——, and R. T. Wetherald, 1967: Thermal equilibrium of the atmosphere with a given distribution of relative humidity. *J. Atmos. Sci.*, **24**, 241–259.

——, and ——, 1975: The effects of doubling the CO_2 concentration on the climate of a general circulation model. *J. Atmos. Sci.*, **32**, 3–15.

——, and ——, 1980: On the distribution of climate change resulting from an increase in CO_2 content of the atmosphere. Submitted for publication in *J. Atmos. Sci.*

——, J. L. Holloway, Jr., and H. M. Stone, 1970: Tropical circulation in a time-integration of a global model of the atmosphere. *J. Atmos. Sci.*, **27**, 580–613.

——, J. Smagorinsky and R. F. Strickler, 1965: Simulated climatology of a general circulation model with a hydrologic cycle. *Mon. Wea. Rev.*, **93**, 769–798.

——, K. Bryan and M. J. Spelman, 1975: A global ocean-atmosphere climate model. Part I. The atmospheric circulation. *J. Phys. Oceanogr.*, **5**, 3–29.

Oort, A. H., and E. M. Rasmusson, 1971: Atmospheric circulation statistics. NOAA Prof. Pap. No. 5, 323 pp. [NTIS COM-72-50295/MF]. [Govt. Printing Office, Stock No. 0317-0045, C55.25.5].

Phillips, N. A., 1957: A coordinate system having some

special advantages for numerical forecasting. *J. Meteor.*, **14**, 184–185.

Ramanathan, V., 1977: Interaction between ice-albedo, lapse-rate and cloud-top feedback: an analysis of the non-linear response of a GCM climate model. *J. Atmos. Sci.*, **34**, 1885–1897.

Roads, J. O., 1978: Numerical experiments on the sensitivity of an atmospheric hydrologic cycle to the equilibrium temperature. *J. Atmos. Sci.*, **35**, 753–773.

Rodgers, C. D., 1967: The radiative heat budget of the troposphere and lower stratosphere. Planetary circulation project, Rep. No. A2, MIT, 104 pp. [NTIS PB-176 527].

——, and D. C. Walshaw, 1966: The computation of infra-red cooling rate in planetary atmospheres. *Quart. J. Roy. Meteor. Soc.*, **92**, 67–92.

Rossby, C. G., and R. B. Montgomery, 1935: The layer of frictional influence in wind and ocean currents. *Pap. Phys. Oceanogr. Meteor.*, **3**, No. 3, 101 pp.

Schneider, S. H., 1972: Cloudiness as a global climate feedback mechanism: The effects on the radiation balance and surface temperature of variations in cloudiness. *J. Atmos. Sci.*, **29**, 1413–1422.

——, 1975: On the carbon dioxide-climate confusion. *J. Atmos. Sci.*, **32**, 2060–2066.

——, W. M. Washington and R. M. Chervin, 1978: Cloudiness as a climate feedback mechanism: Effects on cloud amounts of prescribed global and regional surface temperature changes in the NCAR GCM. *J. Atmos. Sci.*, **35**, 2207–2221.

Schutz, C., and W. L. Gates, 1973: Global climatic data for surface, 800 mb, 400 mb: April. Rep. No. R-1317-ARPA, The Rand Corporation, Santa Monica, CA, 191 pp.

——, and ——, 1974: Global climatic data for surface, 800 mb, 400 mb: October. Rep. No. R-1425-ARPA, The Rand Corporation, Santa Monica, CA, 192 pp.

Smagorinsky, J., 1963: General circulation experiments with the primitive equations: I. The basic experiment. *Mon. Wea. Rev.*, **91**, 99–164.

——, S. Manabe, and J. L. Holloway, Jr., 1965: Numerical results from a nine-level general circulation model. *Mon. Wea. Rev.*, **93**, 727–768.

——, 1978: Modeling and predictability. *Studies in Geophysics: Energy and Climate*. Nat. Acad. Sci., Washington, DC, 133–139.

Stone, H. M., and S. Manabe, 1968: Comparison among various numerical models designed for computing infrared cooling. *Mon. Wea. Rev.*, **96**, 735–741.

Telegadas, K., and J. London, 1954: A physical model for the Northern Hemisphere troposphere for winter and summer. Sci. Rep. 1, Contract AF19(122)-165, Research Division, College of Engineering, New York University, 55 pp. [DOC AD 032472].

van Loon, H., J. J. Taljaard, T. Sasamori, J. London, D. V. Hoyt, Karin Labitzke and C. W. Newton, 1972: *Meteorology of the Southern Hemisphere. Meteor. Monogr.*, No. 35, Amer. Meteor. Soc., 263 pp.

Warren, S. G., and S. H. Schneider, 1979: Seasonal simulation as a test for uncertainties in the parameterizations of a Budyko-Sellers zonal climate model. *J. Atmos. Sci.*, **36**, 1377–1391.

Wetherald, R. T., and S. Manabe, 1975: The effects of changing the solar constant on the climate of a general circulation model. *J. Atmos. Sci.*, **32**, 2044–2059.